A first evaluation of the contribution of aeolian sand transport to lagoon island accretion in the Maldives

Authors / affiliations:

M.J. Hilton[1], D.R. Borrie[1], T.M. Konlechner[2], S.J. Wakes[3], T.P. Lane[4], P.S. Kench[5], D. M. Kennedy[2], Mohamed Aslam[6],

[1]School of Geography, University of Otago; [2]National Centre for Coasts and Climate, School of Geography, University of Melbourne; [3]Department of Mathematics and Statistics, University of Otago; [4]School of Earth Sciences and ARC Centre of Excellence for Climate Extremes, University of Melbourne; [5]Department of Earth Sciences, Simon Fraser University; [6]Small Island Research Centre, Fares-maathodaa, Republic of Maldives.

Corresponding author:

Mike Hilton, School of Geography, University of Otago, PO Box 56, Dunedin 9054, New Zealand (michael.hilton@otago.ac.nz)

ABSTRACT

Aeolian sedimentation and dune development have not been reported from coral atolls at equatorial latitudes. This study presents high-frequency measurements of incident and near surface wind flow and aeolian sand transport on a lagoon sand cay (Maaodegalaa) in the Maldives. Sonic anemometers and Wenglor™ particle counters were operated at 1 Hz for 8 days during the Iruvai monsoon in February 2018. Sand traps were deployed to estimate sand flux and island topography and vegetation cover were surveyed using UAV (un-manned aerial vehicle) photogrammetry and a laser level (in 2017 and 2018). Flow over beach scarps is modelled using computational fluid dynamics.

Maaodegalaa sand cay reaches just 0.9m above the highest spring high tides. Nebkha, between 0.10 and 0.40 m high, are widespread and are associated with *Scaevola taccada* and *Cyperus conglomeratus*. Between 2017 and 2018 the eastern section of the sand cay accreted 0.3 m following *Cyperus* colonisation. Reptation and aeolian ripple development occurred during fieldwork when near-surface flows exceeded 6 ms^{-1}. Saltation occurred at higher wind speeds (8 ms^{-1}). The highest rates of sand transport occurred during north-east incident winds of 12 ms^{-1} (at 6 m), that were probably generated by surface-based density currents under cumulonimbus clouds. Spatially, higher rates of sand transport were recorded downwind of a beach scarp, probably forced by flow acceleration. We propose a conceptual model of lagoon island formation, with both over-wash and aeolian sedimentation contributing to island accretion. A period of aeolian sedimentation may be critical to the emergence of sand cays.

Highlights

- This is the first high-frequency measurement and analysis of incident and near-surface wind flow over a lagoon sand cay in the Maldives and the first to document aeolian sand transport on an equatorial atoll.
- Dune development as the result of aeolian sand transport increased island elevation over a 12 month period.
- Aeolian sedimentation occurs during episodes of high onshore wind speed related to surface-based density currents under cumulonimbus clouds.
- Aeolian sedimentation is enhanced by flow acceleration over beach-scarps cut at spring high tides.

Keywords

Aeolian sedimentation, nebkha, Maldives, island formation, sand cay

Funding sources

[redacted]

Units

1.0 INTRODUCTION

The Maldives is host to approximately 1200 islands located on reef platform surfaces, of which 200 are inhabited (Kench, 2011). The islands are found in two distinct depositional contexts: on the peripheral reef rim of atolls, where the largest islands are situated, and on atoll lagoon reef platforms. All islands are composed of carbonate sand and gravel derived from the surrounding reef. They are typically small in aerial extent and have a mean elevation of less than 1 m above sea-level. Studies of the formation of reef islands in the Maldives have primarily focussed on lagoon islands and have shown the islands are mid-Holocene in age, having accreted vertically as the reef platform grew (Kench et al., 2005; Perry et al., 2012). The formation of the larger vegetated islands occurred during the latter stages of Holocene sea-level rise and its subsequent fall to present level (Kench et al. 2005; East et al. 2018). However, the processes that lead to the emergence of lagoon sand cays above the limit of tides, and the formation of stable islands, both in the Maldives and atolls elsewhere, have not been resolved.

The precondition for island formation, the accumulation of sand as a subtidal sand cay, results from wave processes that transport sediment across the reef flat to a nodal depocentre (Gourlay, 1988; Mandlier and Kench, 2012). Swash processes subsequently control the vertical limit of island building in many reef locations worldwide (e.g. McKoy et al. 2010). In the Maldives, sediment transport fluxes are modulated by seasonal energy gradients, with rapid morphological adjustments occurring in response to monsoonal reversals in wind and wave patterns (Kench and Brander, 2006). At the event scale, extreme waves also impact the islands. For example, the 2004 Sumatran tsunami promoted minor island erosion, but also transferred sediments from beaches to island surfaces. This overwash was able to vertically build the margins of reef islands by up to 0.3 m (Kench et al., 2006).

The potential for aeolian processes to contribute to island formation in the Maldives has not been recognised or assessed. In general, the role of aeolian processes and their potential contribution to island formation in the humid tropics has been underestimated (Hesp, 2008). At lower latitudes, in the southern Indian Ocean, aeolian sedimentation has been shown to contribute to coral island topography, including the Glorioso Islands (Bayne et al. 1970); Tromelin Island (Marriner et al. 2010); the Chagos Group (especially Diego Garcia; Stoddart & Taylor, 1971); and the Cocos (Keeling) Islands (Woodroffe & McLean,1994). A variety of dune forms are reported, including transgressive and sheets, parabolic forms and nebkha. Nebkha are low dunes, convex in profile, formed around vegetation (Pye & Tsoar, 1990). Larger, transgressive dunes reach 11 m in elevation on South Island in the Cocos (Keeling) Islands (Woodroffe, 2008). Parabolic dunes and blowouts are also found in the western Indian Ocean mid-latitude (10^{o} to 25^{o} S) and these are closely aligned with the Southeast Trade winds that persist throughout the year (Schotte and McCreary, 2001). On Tromelin Island wind speeds exceeding 8 m s^{1} are contained in a narrow directional window between 100^{o} and 140^{o} (Marriner et al. 2010). In contrast, the equatorial region of the Indian Ocean, including the Maldives, is an area of relatively low mean wind stress and aeolian sedimentation has not been reported. Indeed, several conditions combine to lower expectations of aeolian activity including the equatorial climate (high humidity, high rainfall, low reported wind speeds); low topography and narrow beach width; and dense vegetation cover on many established islands.

This study arose from the observation of aeolian ripples, shadow dunes and nebkha on Maaodegalaa sand cay by the authors during fieldwork in February 2017. Considering most lagoon sand cays are little more than 1 m above the reach of spring tides, any dune development may significantly contribute to island relief. Remarkably, the key process mechanisms that build islands above sea-level, including the development of a stable cay surface, which can then be colonised by plants, remain to be investigated. Sand cays and islands occur in a range of forms in the atoll lagoons of the Maldives, from submerged sand cays, to recently emerged cays colonised by early successional vegetation, to stable and forested islands. The current paper reports the first measurements of aeolian sedimentation in the Maldives on a low-lying sand cay (Maaodegalaa) in Huvadhoo Atoll. We aim to (i) measure incident and near-surface wind flow and associated aeolian sand transport over a recently emerged sand cay; (ii) examine spatial variations in patterns of sedimentation, particularly processes of flow acceleration and sediment transport over beach scarps; and (iii) consider the implications of aeolian sedimentation for island formation.

2.0 REGIONAL SETTING

The Maldives comprises a double chain of atolls which extends almost 900 km, from 6^{o} 57' N latitude, to just south of the equator (0^{o} 34' S latitude). Huvadhoo atoll, just north of the equator, is the largest atoll in the Maldives (Figure 1), with an area of 3,279 km^2 and maximum dimensions of 80 km (north-south) and 60 km (west-east). The rim of the atoll is defined by reef platforms and islands, broken by multiple deep channels. The atoll lagoon, which attains water depths of 80 m, contains (i) patch reefs and (locally) 'faros' (donut-shaped reefs with a central depression); (ii) patch reefs with ephemeral sand deposits covered at spring high tide; (iii) sand cays on reef platforms that rise above the reach of spring high tides, and which have an early successional vegetation cover (locally 'finolhu'); and (iv) forested islands. The lagoon contains 71 patch reefs and 25 faros. A further 39 islands are long established, as indicated by a tall forest cover. Sand cays occur on 30 of the lagoon platforms – of which 27 appear to be overwashed by waves at high tide (as suggested by the absence of vegetation and wrack in aerial photographs and satellite images) and three are emergent and vegetated. The vegetation type on these sand cays is early successional – primarily the shrub *Scaevola taccada* and the sedge *Cyperus conglomeratus*. Maaodegalaa Island is an example of the emergent sand cay type. Comparisons of recent satellite imagery indicates the position and plan form of submerged and vegetated sand cays is highly dynamic. Maaodegalaa, for example, has only occupied its current position for 8 years (since 2011) and was unvegetated in 2006 (see Supplementary Material).

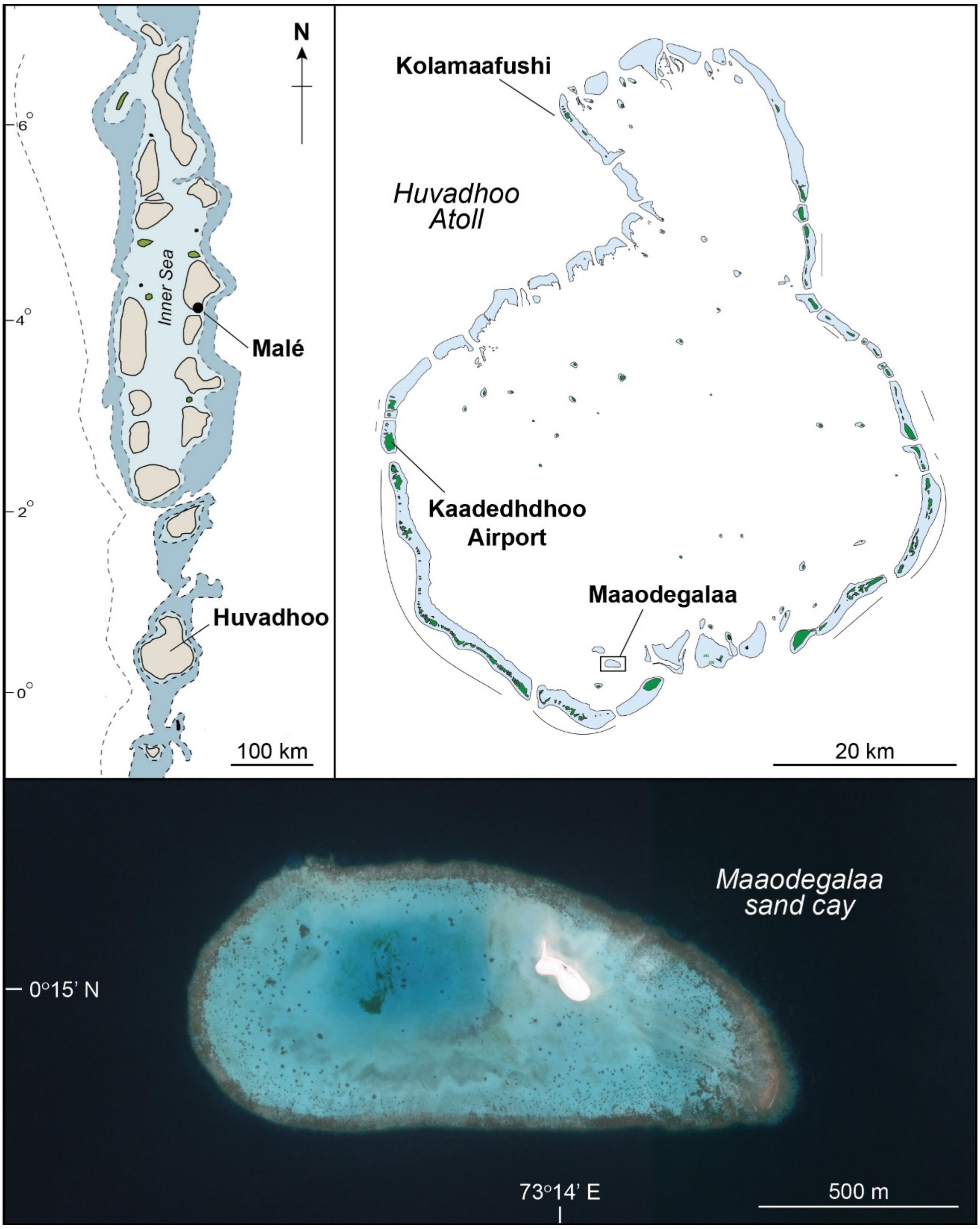

Figure 1: The study site is a coral sand cay in the southern section of the lagoon of Huvadhoo Atoll in the southern Maldives. Long-term climate data reported is from Kaadedhdhoo Airport and tidal predictions are from Kolamaafushi Island. The satellite image is courtesy Google Earth (19th February 2014).

All lagoon sand cay and island forms in Huvadhoo Atoll are composed of sand-size carbonate sediments, primarily fine to medium coral sand (Liang et al., 2016). Sand cays are perched on the near-level reef platform surface, which allows islands to shift position on the platform in response to variations in swell and local waves (Aslam & Kench, 2017). The fully vegetated islands have a forest cover of plantation (*Cocos nucifera*) and/or native tree species (e.g. *Pisonia grandis*, *Calophyllum inophyllum*), and are relatively stable in position on the platform.

The wave and wind regime of the Maldives is dominated by the Indian Monsoon Reversal (Figure 2A). Tropical cyclones are rare and mainly affect the northern atolls. Only five cyclones have occurred between 0^{o} and 5^{o} N latitude, at 73^{o} E longitude, since 1945 (http://www.nhc.noaa.gov/data). Strong seasonal wind patterns are associated with the east-northeast (Iruvai) monsoon (December to March, 045^{o} - 090^{o}), and the southwest (Hulhangu) monsoon (April - November, 225 - 315^{o}). Mean wind speeds at Kaadedhdhoo Airport on the western rim of Huvadhoo Atoll (at 9am) are 3.08 m s^{1} during Hulhangu and 2.45 m s^{1} during Iruvai (Figure 2b). Data on the maximum near-ground wind speeds in Huvadhoo Atoll is poor, but indicates that there is little difference between average monthly and average maximum monthly (9 am) wind speeds. Average maximum monthly (9 am) wind speeds are just 2 m s^{1} higher during the Hulhangu. Precipitation increases from north to south as the influence of the monsoon decreases (Storz and Gischler, 2011). Average annual precipitation for Huvadhoo is 2,651 mm, with the lowest rainfall (50 - 100 mm / month) occurring in the Iruvai months of February and April and with rainfall of between 150 and 250 mm during the rest of the year (Gan data, 2000-2018, Maldives Meteorological Service).

Waves in the lagoons of the Maldives atolls are both locally generated, fetch-limited waves, and distance-source swell that propagate into the lagoon through channels between the rim islands. On a seasonal basis, swell propagates from the southeast from December to February (Hulhangu) and is characterised by significant wave height and period of approximately 1.2 m and 8.5 s, respectively. During April – November (Iruvai) swell propagates from the south and is characterised by longer wave period (10.5 s) and a

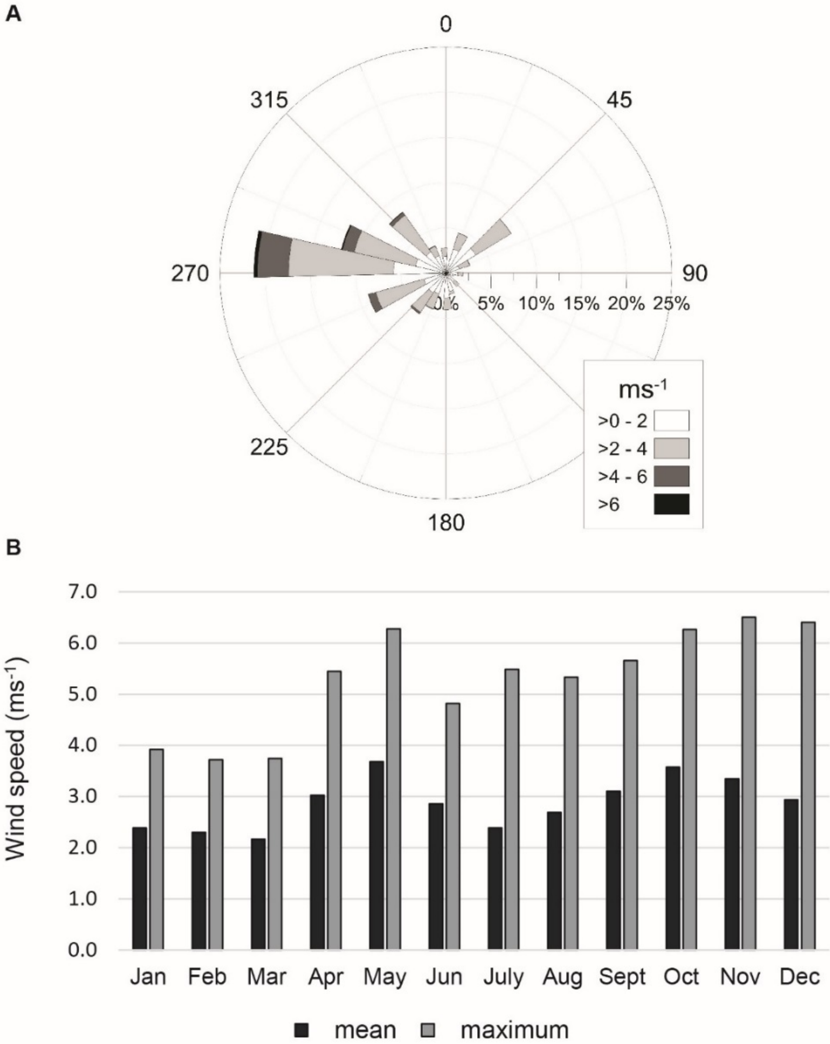

Figure 2: (A) Wind rose and (B) mean monthly wind speed and maximum monthly wind speed at Kaadhedhdoo Airport (Maldives Meteorological Service, 9 am data, 10 m mast, 1991 – 2008).

significant wave height above 1.5 m, peaking at 1.95 m in July (Kench et al. 2006). Maaodegalaa is situated close to a gap in the rim of Huvadhoo Atoll, and is likely affected by the prevailing southerly swell, but is relatively sheltered from short period waves within the lagoon by the rim islands to the west. Conversely, Maaodegalaa is relatively exposed to lagoon waves from the northeast.

Surface waves result in occasional island inundation. Long period swell events, driven by high latitude storms, resulted in rim island inundation in the southern Maldives in 1987 and 2007 (Harangozo, 1992). Wadley et al. (2017) examined two significant flood events that resulted in island inundation in the Maldives (10^{th} –13^{th} April 1987 and 15^{th} – 17^{th} May 2007). They concluded that coastal flooding in the Maldives is most likely to occur during long-period (up to 20 s) energetic waves generated in the Southern Ocean combined with spring tides. A swell event affected the southern atolls of the Maldives on the 20^{th} and 21^{st} April 2018, when an intense low-pressure system lay 1000 km to the southeast of the Maldives (Maldives Meteorological Service Advisory issued 26^{th} April 2018). Finally, the Indian Ocean 2004 tsunami inundated the eastern margins of rim and lagoon islands in South Maalhosmadulu Atoll, depositing sand sheets on island surfaces to a maximum depth of 0.3 m (Kench et al. 2007). Tides in the study area are semi-diurnal with a spring tide range of 1.2 m. There is little to no potential for pressure-forced storm surge, since sea-surface atmospheric pressure only varies 2-3 hPa around the mean pressure (1010 hPa) (Kaadedhdhoo Airport hourly data, 2012 – 2016, Maldives Meteorological Service).

3.0 MATERIALS AND METHODS

The current study reports observations and measurements of aeolian sedimentation on Maaodegalaa sand cay, Huvadhoo Atoll, over an 8-day period in February 2018 during the northeast monsoon and island accretion and dune development over a 12 month period

(January 2017 – February 2018). The lagoon islands of the Maldives are comprised of biogenic materials (Liang et al. 2016) but there was no existing information on the textural characteristics of Maaodegalaa. Surface sediment samples (0 – 0.05 m) were collected by hand around the island from the beach toe (n = 18), mid-tide level (n = 18), and across the supra-tidal island (n =58). Samples were washed, split and analysed, using a Beckman Coulter LP13320 Laser Particle Analyser.

Sea-level was recorded continuously during fieldwork using a single RBR Duet pressure transducer approximately 80 m northeast of Maaodegalaa sand cay on the reef platform. Local, fetch-limited waves, formed within the lagoon, were not directly measured, but short-period (2 - 5 s) breaking waves, primarily from the north, did not exceed 0.3 m at high tide. Island morphology was surveyed in February 2017 and February 2018, using a Sprinter auto level, unlike marked transects (A – C, Figure 3), with all points (and the RBR data) reduced to a common vertical datum (WGS84 EII) established using a Trimble RTK-GPS. Three-dimensional island morphology, and an orthomosaic of the island surface, were derived from UAV (Phantom-3 Advanced) imagery using Drone-deploy™ flight control and PIX4D™ post-processing software. Ground control points were not used to georeference the orthomosaic - the internal GPS of the UAV was used for positional accuracy. The relative accuracy of the derived elevations, + / - 10 cm, was estimated by comparing the contours derived from the UAV photogrammetry with profile elevations.

Observations of incident and near-bed wind flow and associated sedimentation were made between the 27thJanuary and the 4th February 2018 at two sites on the sand cay (Figure 3 & Figure 4). Incident wind was measured above the cay on a 5.5 m mast. Wind speed and direction were recorded (at 1Hz) using Gill Windsonic-2D sonic anemometers and Campbell CR1000 data-loggers. Velocity profiles derived during the first four days of fieldwork (when the mast supported anemometers at 0.05, 0.50 and 5.53 m) indicate the highest anemometer was located above the boundary layer. Sediment transport as saltation was recorded using Wenglor™ laser particle counters with the laser set at 0.01 m above the bed, anticipating particle transport rates well below 700 Hz (Bauer et al. 2018). Total near-bed sand flux was determined by deploying a network of swinging sand traps (described in Hilton et al. 2017) positioned 1 cm above the bed.

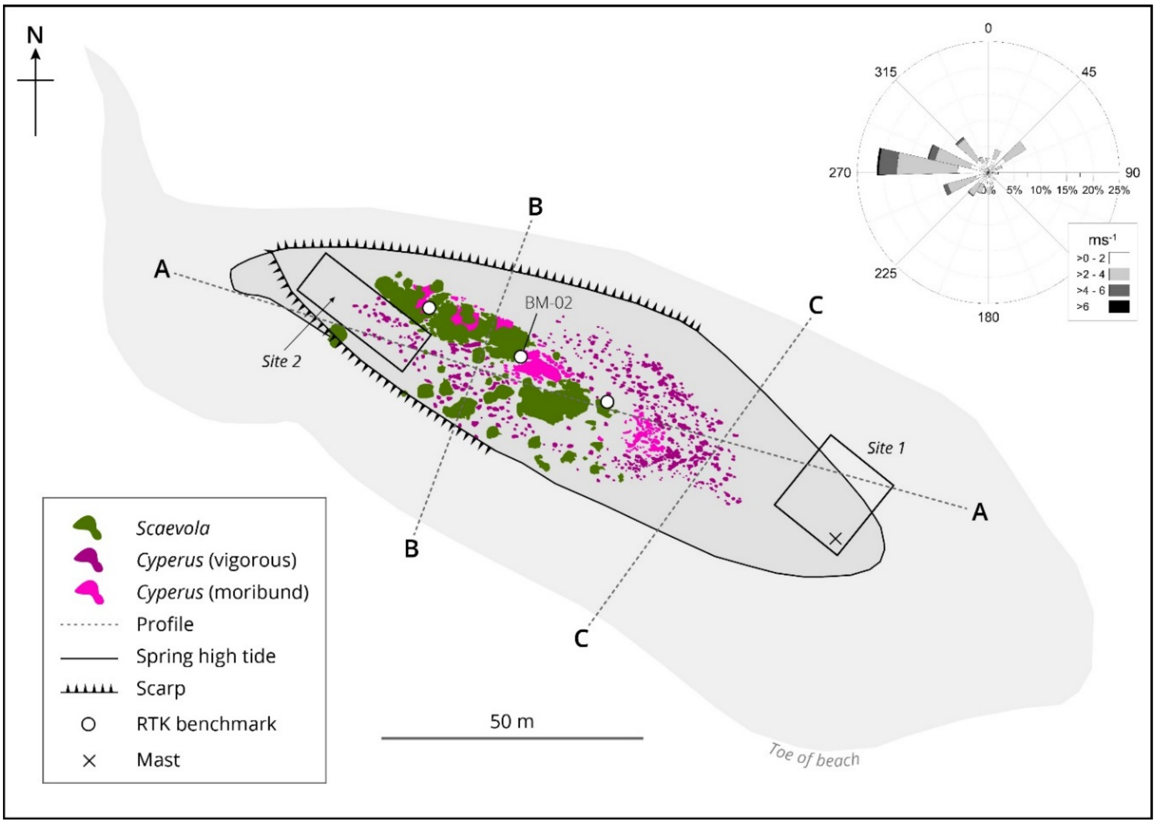

Figure 3: Location of surveyed transect lines (A-C) on Maaodegalaa sand cay, anemometer mast (5.53 m), benchmarks, and the sites instrumented during the two wind events reported. The extent of the two main plant species, *Scaevola taccada* and *Cyperus conglomeratus* (vigorous and moribund); and the back-beach scarp cut by spring high tides (following spring high tides on the 31st January 2018) are mapped. The inset wind rose (0900 hrs observations, 1991 – 2008 at Kaadedhdhoo Airport) indicates the north coast of the sand cay is relatively exposed to wind and local wind waves during the Iruvai Monsoon.

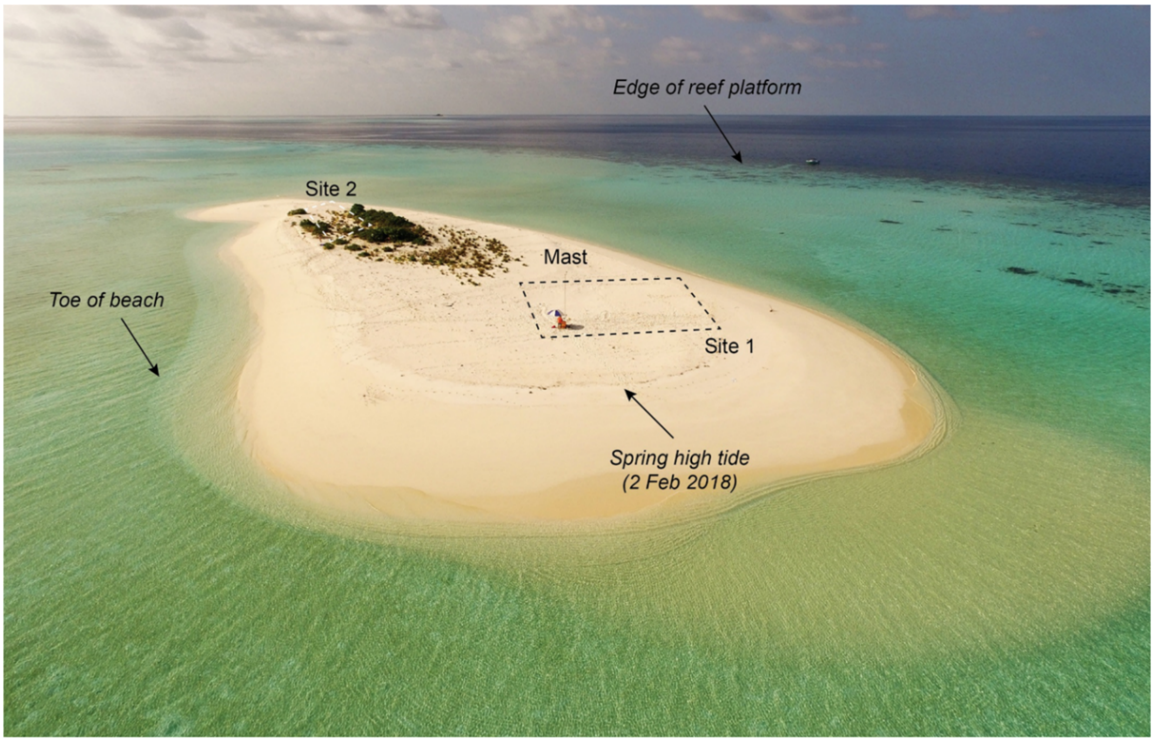

Figure 4: UAV aerial oblique view of Maaodegalaa Island (looking to the west) showing instrumented areas during Event 1 (site 1, 28th January 2018) and Event 2 (site 2, 1st February 2018); and the location of the anemometer mast (adjacent to the sun umbrella) for the period 27th January to 3rd February 2018.

Site 1, at the eastern end of the island is an unvegetated sand terrace with a gently-sloping convex profile, c. 0.50 m above spring high tide and 0.20 m above the surveyed limit of wave swash at spring high tide (Figure 4). The area was cleared of wrack and raked smooth on the 27th January after instruments were installed. The unvegetated fetch to the northwest of the instrument array was 60 m. A community of *Cyperus*, a 0.3 – 0.4 m high plant with a tussock growth form, was located 30 - 40 m to the west of the mast. Instruments and sand traps were arranged in lines at 90 ° (043° relative to true north) to the forecast wind direction during the first few days of the deployment (Figure 5).

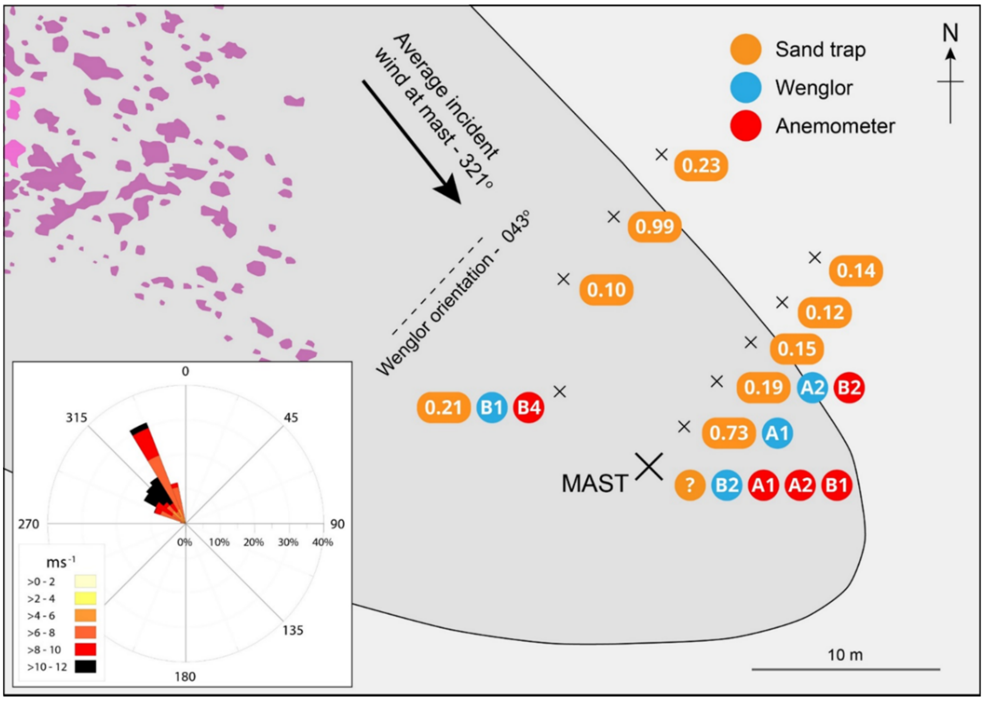

Figure 5: Site 1 instrument layout during Event 1 (from 1800 hours, 28th January 2018). The Wenglor particle counters were oriented at 288° prior to the event, 033° from normal to the average incident wind for the event (321°). The wind rose indicates wind speed and direction at A1 (5.53 m). The values in the sand trap symbol indicate the weight (g) of sand trapped in the period 1500 hours on the 28th January to 0900 hours on the 29th January.

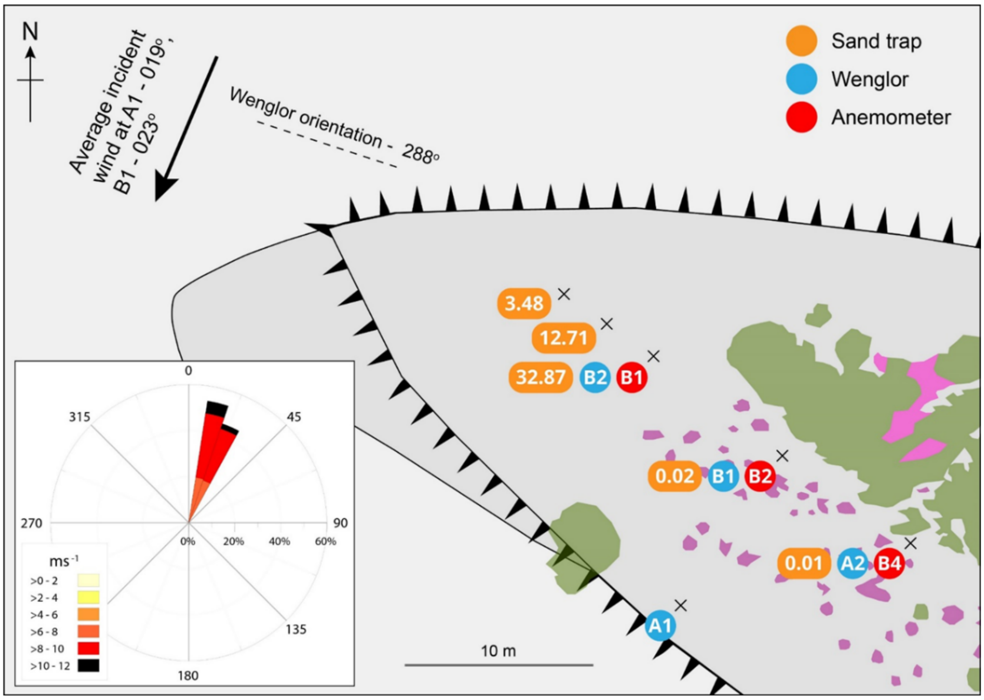

Figure 6: Site 2 instrument layout during Event 2 (1300 hours, 1st February 2018). The wind rose represents incident wind speed and direction at A1 (5.53 m). The values in the sand trap symbol indicate the weight (g) of sand trapped in the period 1300-1320 hours.

Site 2 was at the north-western end of the island on a flat terrace bounded by back-beach scarps to the southwest and north (Figures 4 and 6). This scarp was observed on arrival on the island on the 27th January, but it was refreshed during spring high tides that reached their maximum elevation on the 1st February 2018. The instruments and sand traps at site 1, with the exception of the mast and anemometer A1 (5.53 m), were shifted to site 2 on the 1st February. A Wenglor (B2) and anemometer (B1) were located 9 m from the edge of the scarp along the northern side of the island. Fortuitously the incident wind direction on the afternoon of the 1st February crossed the scarp at an angle of 023^{o} and close to normal (95^{o}) to the long-axis orientation of Wenglor B2. The remaining instruments were installed in the lee of a line of *Scaevola* and were relatively sheltered from onshore winds during a second wind event.

During fieldwork we hypothesized that back-beach scarps (Figure 7) were accelerating wind flow and enhancing sedimentation. We noted the presence of a strip of rippled fine sand adjacent to and downwind of the beach scarp along the north coast of the sand cay, which we reasoned was a depositional surface; but not an overwash surface, since it was free of wrack. Two-dimensional Computational Fluid Dynamic (CFD) simulations of wind flow were subsequently undertaken over the scarped (Profile B, Figure 3) and un-scarped (Profile C) transects across the island to examine the influence of the beach scarps on near-bed flow acceleration. We employed SIMPLE discretisaton scheme and the solver ANSYS Fluent™. A mesh density study was undertaken with a final mesh of approximately 500,000 cells. The smallest cell employed, closest to the ground, was 0.02 m. The two-equation Renormalisation Group (RNG) k-□ Reynold Averaged Navier-Stokes (RANS) turbulence model was used. The domain was 100 m long by 45 m high with a top symmetry boundary condition and pressure outlet. The 8 m s^{1} incident wind profile was developed in a separate simulation over sea of roughness height value of 0.0125 (Perianez, 2004). The bottom surface was the island covered in sand with sea either side. The profile transect was taken at low tide, from the Sprinter survey data, and had a sand roughness height value of 0.05 m (Wakes et al. 2010).

Figure 7: Spring high tides during the period of fieldwork eroded the base of a pre-existing beach scarp (mapped in Figure 3). This photograph shows the presence of ripples and shadow dune features along the edge of the terrace behind the scarp. The photograph (on Profile B) was taken on the 28th January 2018. The highest spring tide on the 1st February overtopped the scarp.

4.0 RESULTS

4.1 Sediments

The island is composed of fine to medium, moderately-well sorted, reef carbonates. Surface samples from the reef platform, obtained approximately 5 m from the toe of the beach, are relatively coarse and less well sorted (mean grain size = 0.42 +/- 0.65 phi units), compared with the intertidal beach at mean tide level (0.96 +/- 0.57 phi) and the supratidal island surface (1.34 +/-0.51 phi). Visual inspection of the sediments indicated they were composed of almost entirely of coral species, with *Halimeda sp.* and *Foraminifera sp.* detritus comprising a small proportion of intertidal and beach toe samples. Most of the grains were semi-spherical, but angular. Whole clasts of *Helimedia* were found in samples from the beach toe but were not found in supratidal samples. Estimates of bulk density for samples taken above spring high tide average 1.60 g cm^3, which is 60 percent of the density of quartz (2.65 g cm^3).

4.2 Sand cay topography and aeolian features

The highest point on Maaodegalaa sand cay is approximately 0.9 m above spring high tide and 0.7 m above the limit of wave swash at spring high tide on the 1 February 2018 (Figure 8). The spring high tides from the 31st January to the 2nd February were the highest tides experienced during 2018 (Kolamaafushi tide tables, 65km north of Maaodegalaa, Figure 1), and only 0.01 m below the highest astronomical spring high tides. The highest parts of the island are vegetated (Figure 8), with communities dominated by *Scaevola* or *Cyperus*, except for a low (unvegetated) ridge (0.30 m high) to the east of the *Cyperus* community. A central ridge, oriented north-west to southeast, and parallel to the long axis of the island, is associated with *Scaevola* (Profile A, Figure 9). A second line of *Scaevola*, comprising lower and probably younger plants (<1 m), associated with nebkha, runs parallel to the central ridge along the south coast of the island.

Nebkha occur in two forms: (i) small discrete nebkha formed with individual specimens of *C. conglomeratus*; and much larger nebkha formed around *Scaevola* along the southern shoreline (Figure 9). The former occur on surfaces recently colonised by *Cyperus* and form small isolated pedestals of sand trapped within the tussock growth form of this species. Individual nebkha are small, barely 0.40 m wide, and less than 0.40 m high (Figure 9A). But they are widespread across the eastern half of the sand cay and south of the main areas of *Scaevola* (Figure 8). These dunes, aeolian ripples and shadow dunes, were observed during our first visit to Maaodegalaa in January 2017 (Figure 10). The morphology and orientation of the larger nebkha – the long axis is oriented southwest to northeast - suggests sediment transport and dune formation occurred during southwest winds.

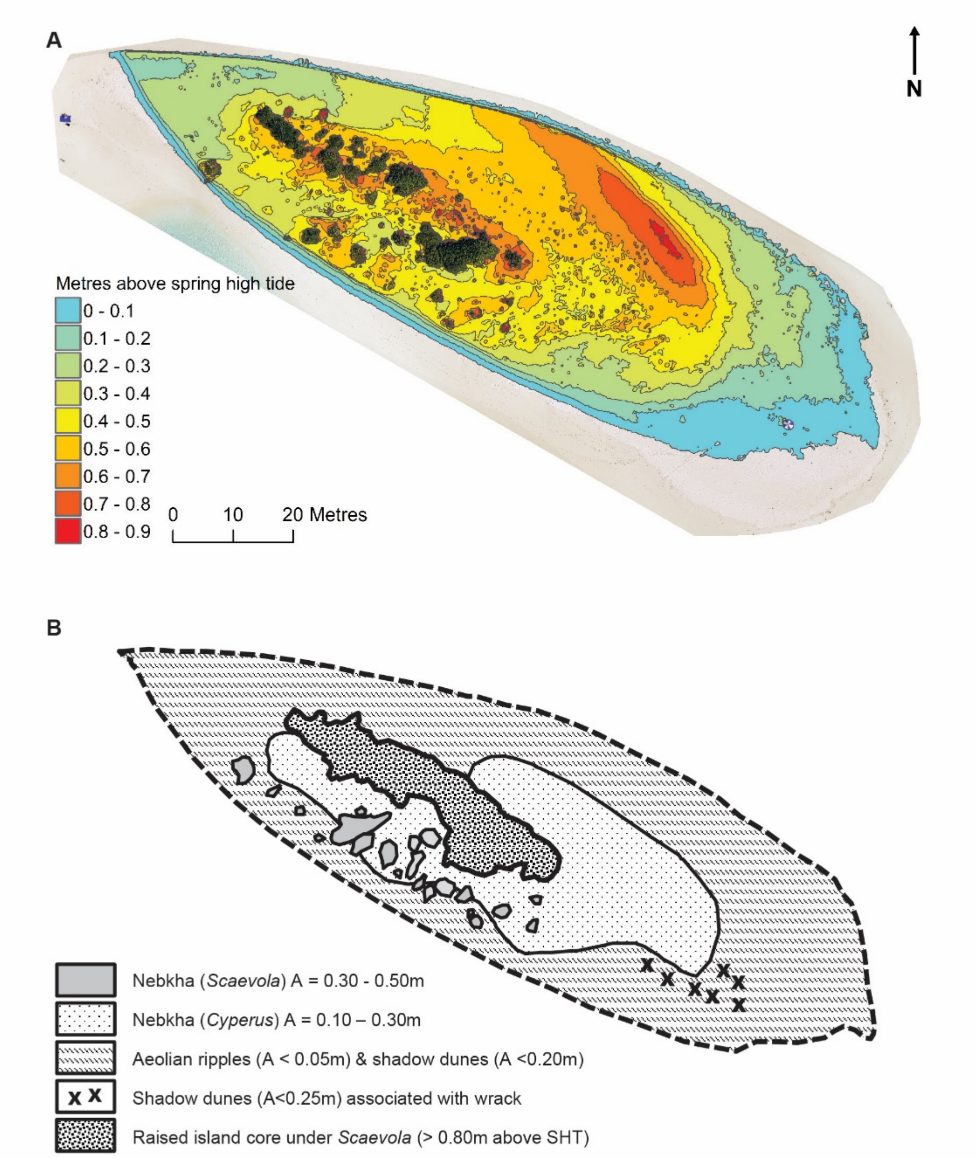

Figure 8: (A) The topography of Maaodegalaa derived from UAV photogrammetry (30th January 2018) relative to spring high tide; and (B) an interpretation of aeolian features. Nebkha along the southern margins of the island are associated with Scaevola. Smaller nebkha, associated with Cyperus, extend to the east of the island core vegetation and (to a lesser extend) occur with Scaevola along the south coastline. Aeolian ripples were observed on all unvegetated surfaces, particularly the western, eastern and northern unvegetated surfaces.

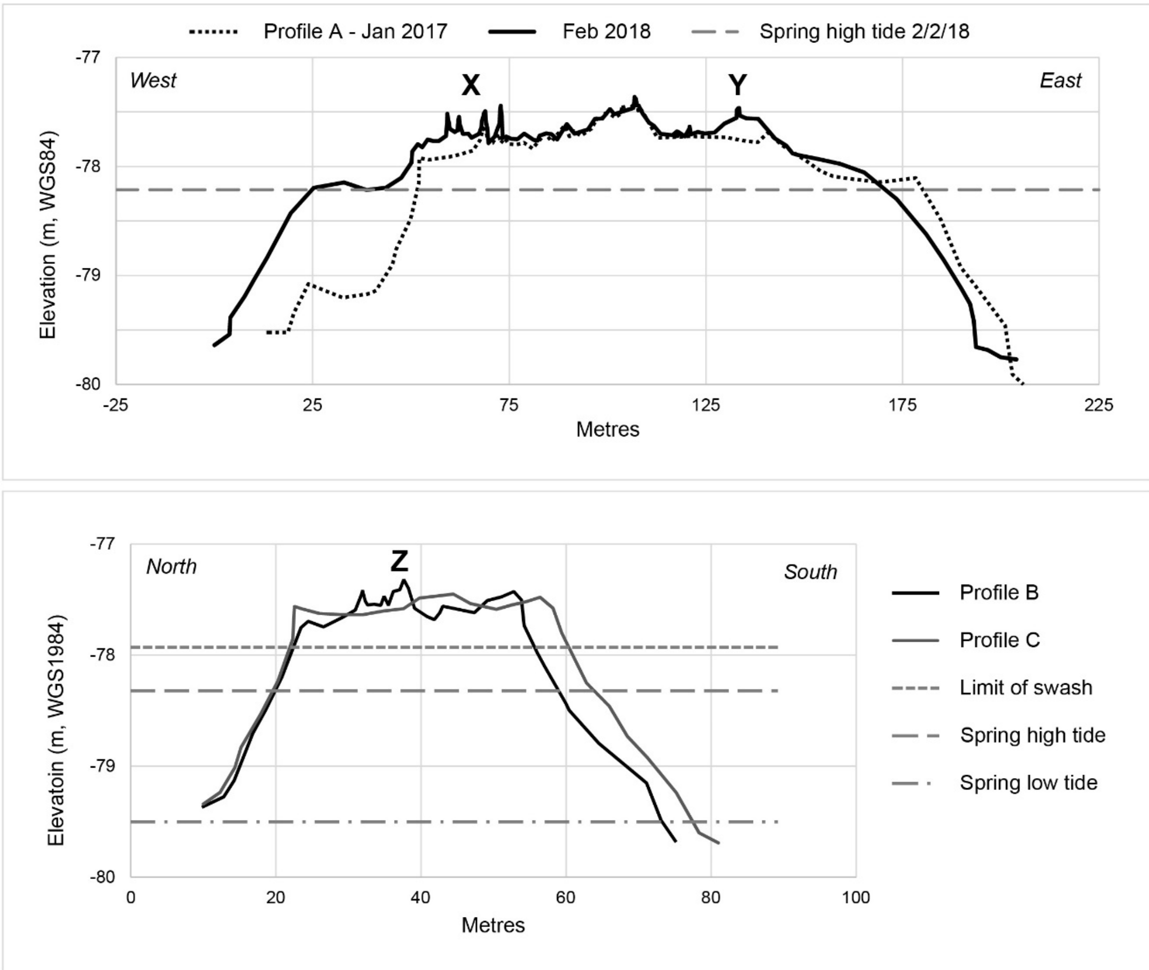

Figure 9: Profiles A-C surveyed across Maaodegalaa in January 2017 and February 2018 (Profile A only) (located in Figure 3). Areas of high topography are associated with small nebkha (X, see Figure 10B) and larger nebkha formed in association with *Scaevola taccada* (Z, see Figure 10C). Between January 2017 and February 2018 the eastern terrace of the island, formerly unvegetated, accreted in association with a new community of *Cyperus conglomeratus* (Y).

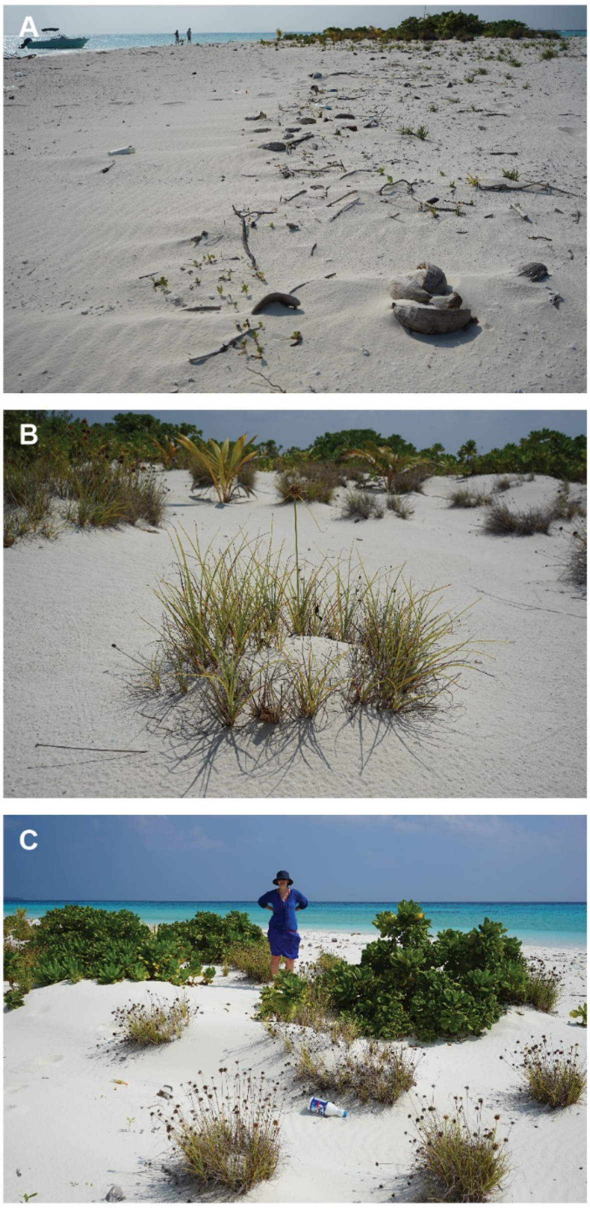

Figure 10: Aeolian features on Maaodegalaa sand cay in February 2017: (A) aeolian ripples and shadow dunes formed in the lee of wrack (flow right to left, north to south); (B) minor nebkha (height < 30 cm) associated with *Cyperus conglomeratus*; and (C) larger nebkha (height < 50 cm) associated with *Scaevola taccada* (near the western end of the island).

Two areas, to the west and east of the core of the sand cay, accreted between fieldwork in January 2017 and February 2018 (Figure 9). *Cyperus conglomeratus* established in both of these areas in late 2016 and were present as seedlings in January 2017, which had matured by February 2018 (Figure 11). We surmise that aeolian sedimentation contributed to this accretion since there was no evidence of fresh wrack within the *Cyperus* community in February 2018, which would indicate overwash. The “high” ridge evident in Figure 8, which lies at an oblique angle to the northeast shoreline, 0.20 – 0.30 m high, is the only elevated surface not associated with vegetation.

The current form and location of Maaodegalaa on the reef platform established between February 2011 and March 2013 (see supplementary data). Maaodegalaa has been relatively stable in both form and position on the reef platform since 2013, although the supratidal area of the island has reduced since 2016. Prior to 2013, between the first available satellite image (2006) and 2014, the island experienced major changes in location, form and vegetation cover. The centre of the sand cay in 2010 was located over 50 m to the north of the current midpoint, although there is some overlap between the footprints of the cay in 2010 and 2018. Consequently, elements of the topography of the current cay are likely to be inherited from periods when the island had a different plan form and exposure to waves and incident winds. The potential for aeolian sedimentation and dune development must have also changed as the dry sand fetch (relative to the current vegetated island core) has changed. In 2006 the sand cay was unvegetated. This fetch extended further to the north in 2010 and to the west in 2016. The cay in February 2018 was narrower and more elongated, compared to its form in 2014. The vegetated core of the cay has been stable only since 2014 (or since the cay was recolonised by vegetation after the cay migrated south between 2011 and 2013). The unvegetated ridge referred to above is an anomaly - all other elevated areas comprise nebkha formed in association with vegetation. It may be a relict feature inherited from an earlier island configuration and vegetation cover. Finally, we assume, but have not verified, that the vegetated core of the island accreted by a combination of aeolian and overwash deposition.

Figure 11: UAV images of Maaodegalaa in January 2017 (courtesy Eddy Beetham) and March 2018. Areas of accretion on the eastern terrace and the western margins of Maaodegalaa are associated with *Cyperus conglomeratus* and the formation of *Cyperus* nebkha over a 13 month period (January 2017 – February 2018).

Wrack is scattered across the eastern half of the island (Figure 10A), at elevations up to 0.5 m above spring high tide and 0.3 m above the observed limit of swash. This material comprises plastics, fishing and household items, as well as seeds (with coconut husks conspicuous) and other natural organic debris. Wrack is not present across the western half of the island, including the area of larger nebkha along the south coast of the island (Figure 10 and Figure 11d). The low terrace east of Profile B must be subject to occasional inundation, given the presence of relatively fresh wrack. This wrack introduces a significant roughness element to the surface resulting in shadow dune development. It also contains the seed of early successional marine-dispersed plants (such as *Cyperus conglomeratus*), which suggests sand cay accretion results from a combination of wave overwash, plant colonisation, aeolian sedimentation and dune develop.

4.3 Incident and near-surface wind flow

The mean incident wind speed at A1 (5.53 m) during the 8-day instrument deployment was 4.55 m s^{1}. The highest speed recorded was 12.84 m s^{1}; however, wind speed generally ranged between 1 – 7 m s^{1} and it was only momentarily calm on the 31st January. Wind direction was generally from the northwest to the northeast (Figure 12), consistent with the Iruvai monsoon, apart from a period of low-speed southwest wind (31st January). Two periods of high wind speed were recorded - hereafter ‘Event 1’ and ‘Event 2’. Each lasted about 60 minutes – Event 1 commenced around 2000 hrs on the 28th January and Event 2 around 1300 hrs on the 1st January 2018 (Figure 12a-c). Abrupt increases in wind speed occurred during each event, accompanied by changes in incident wind direction. During the first event wind speed at A1 increased by approximately 7 m s^{1} to 12.84 m s^{1}, with a direction at the time of the peak wind of approximately 340° and then shifting to northerly (020°) later in the event, a shift in wind direction of approximately 40^{o} (Figure 13). During Event 2, the wind speed at A1 increased by approximately 8 m s^{1} to 11.45 m s^{1}, from a bearing of 020^{o} with a net change in wind direction during the event of 75^{o} (Figure 14).

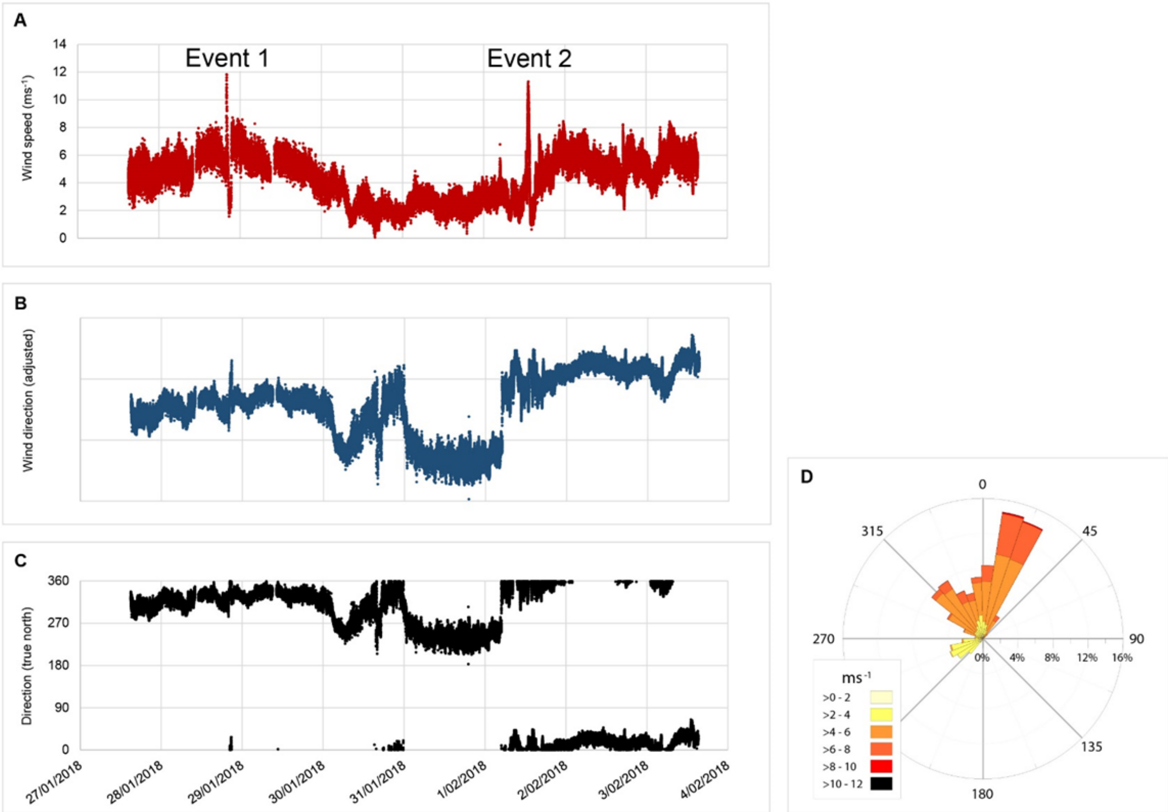

Figure 12: Maaodegalaa (A) wind speed; (B) relative wind direction; and (C) wind direction (true north); and (d) wind rose, for the period 27th January to the 3rd February 2018 (at 5.53 m (A1) on the mast).

The equatorial and isolated location of Maaodegalaa sand cay means that most weather systems or terrain-generated phenomena are unlikely candidates for generating these wind events, leaving moist convective activity as a potential cause. Satellite imagery and satellite-derived rainfall products (e.g., NOAA CPC Morphing Technique - CMORPH data, not shown here) identified convective activity and rainfall near Maaodegalaa during both events. Specifically, for Event 1 there were isolated storms in the area and rainfall detected two hours before and a few hundred kilometres to the north of Maaodegalaa. For Event 2 the satellite images show a large convective complex approaching Maaodegalaa from the northeast, and we photographed large and classic cumulonimbus clouds close to the island at the time of the event.

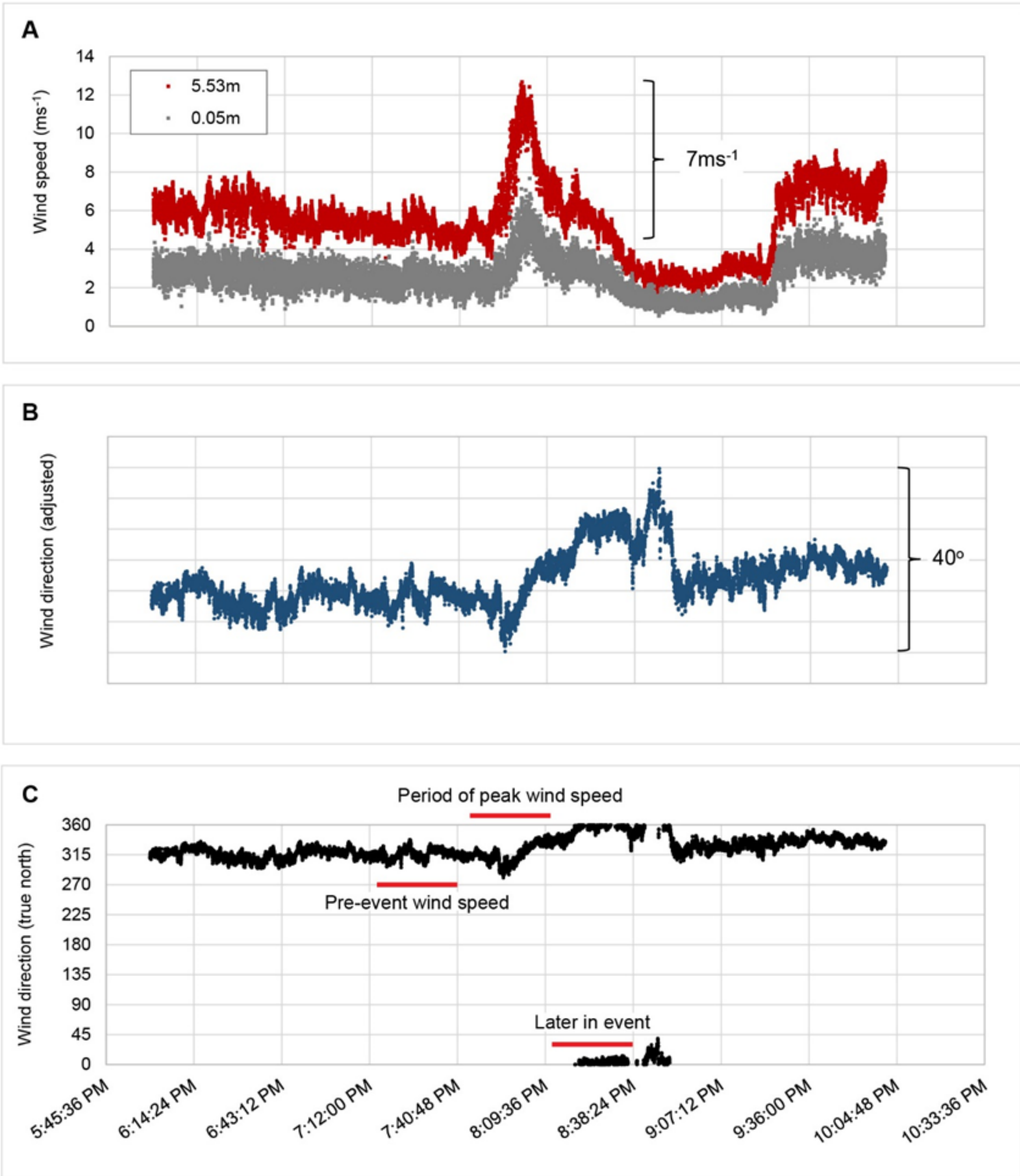

Figure 13: (A) Wind speed; (B) wind direction (adjusted); (C) wind direction (relative to true north) at 5.53 m (A1, mast) and at 0.05 m (B1, base of mast) during wind Event 1 (28th January 2018).

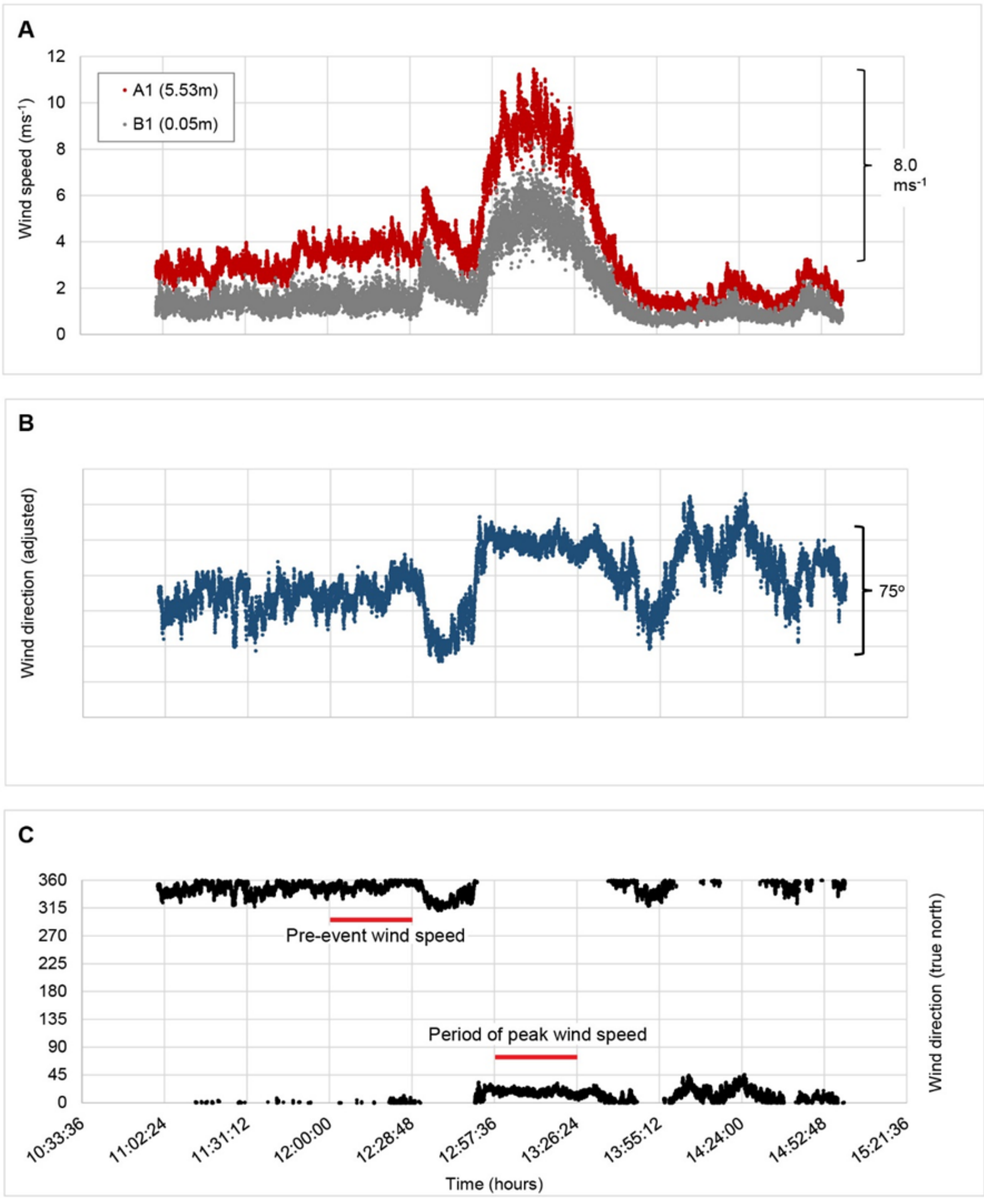

Figure 14: (A) Wind speed; (B) wind direction (adjusted); (C) wind direction (true north) at 5.53 m (A1, mast) and at 0.05 m at the western end of the island (B1) during Event 2 (1st February 2018).

Precipitating convective clouds produce surface-based density currents (or ‘cold pools’) associated with the evaporation of rainfall and are prominent features of thunderstorm environments (e.g., Houze 2004, and the references therein); can typically have wind strengths of 10 m s^{1}; and can travel for significant distances if unimpeded by topography -

especially when generated by mesoscale convective systems. It is likely that cold pools are responsible for the wind shifts measured during Events 1 and 2. First, the strength and duration of the wind perturbations are consistent with other studies of tropical cold pools (e.g., Feng et al. 2015). Second, the direction of the wind shift is consistent with propagating cold pools originating from the locations of the satellite-observed rainfall relative to Maaodegalaa. Third, (low quality) temperature measurements (Campbell CR1000 dataloggers used during fieldwork) identify distinct reductions in temperature of 3^{o} C at the time of the wind shift (not shown). Finally, following the passage of the strongest part of each shift there is a notable reduction in wind variability (gustiness), signifying a change in air mass, which is consistent with the stabilisation of the boundary layer following the passage of a cold pool. However, without additional high-quality measurements (temperature, pressure, and relative humidity) it is impossible to determine unambiguously whether these features resulted from thunderstorm-generated cold pools.

4.4 Aeolian sand transport during Events 1 & 2

Saltation was observed in each of the experimental areas during the two periods of high wind speed described above. During Event 1 the incident wind crossed a dry unvegetated sand surface with a fetch length of 50 m (Figure 5). The fetch decreased to 20 m as the shore-parallel incident winds shifted towards the north and became less oblique onshore. Wind speed exceeded 12 m s^{1} at A1 (5.53 m) and 6 m s^{1} at ground level (B4, 0.05 m) during the event. Wind direction shifted from 290^{o} at the commencement of the event to 340^{o}. Saltation was poorly developed and the Wenglor particle counters recorded low counts (< 8 counts s^{1}). Wenglor A2, located closer to the north coast of the island (Figure 5), recorded somewhat higher counts (Figure 15). Sand transport occurred primarily as reptation during this event, since ripples (length = 0.12 m, amplitude = 0.03 m) and shadow dunes formed around our equipment overnight. Saltation did occur, however, as recorded by the Wenglors and small quantities of sand was trapped in the swinging traps (0.10 - 0.73 g, Figure 5). These traps were set 0.01 m above the bed, so the derived flux for the duration of the event (if we assume sand transport only occurred during Event 1) ranged between 65.75 – 479.95 g / hour / m^2.

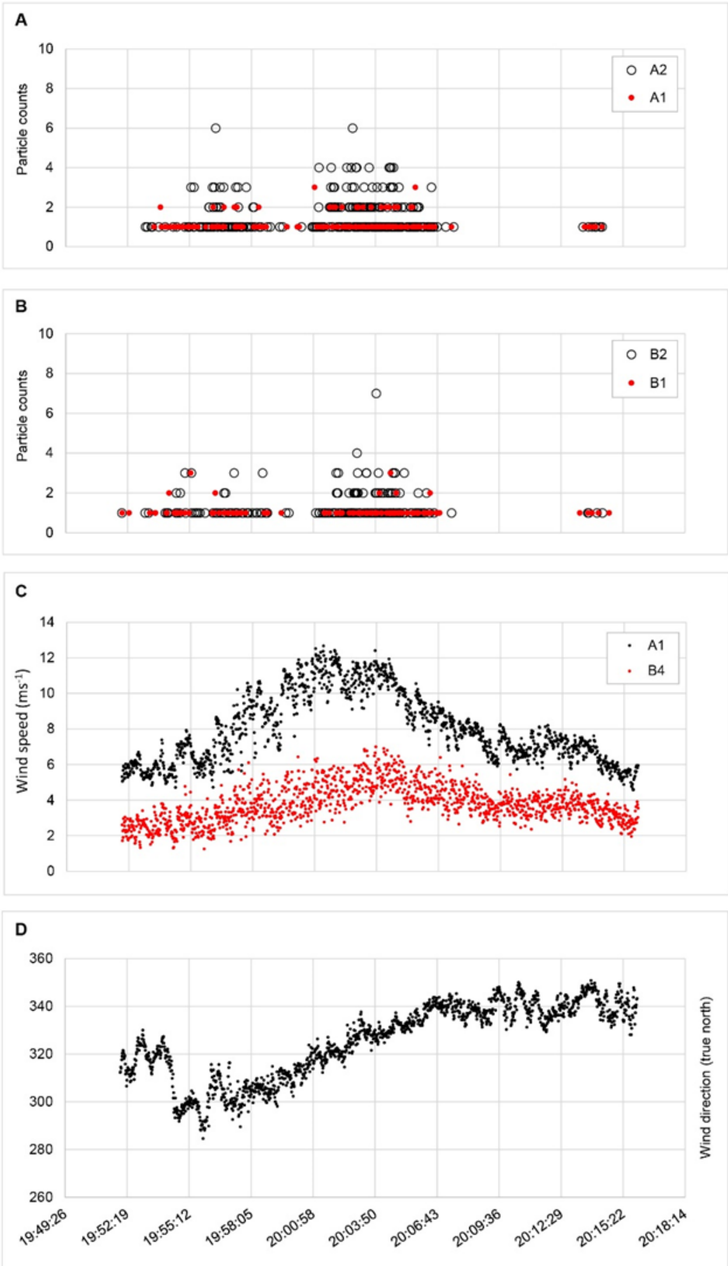

Figure 15: Wenglor particle counts at sites (A) A1 / A2 and (B) B1 / B2; (C) wind speed (A1, 5.53 m and B4, 0.05 m); and (D) wind direction (A1) during Event 1 (28th January 2018).

Higher levels of saltation were recorded by the Wenglor particle counters during the second wind event (0 -160 counts s^{1}) (Figure 16). Maximum incident wind speeds (measured at 5.53

m (A1) on the mast) were lower during Event 2 (11.6 m s^{1} compared with 12.8 m s^{1} for Event 1), however, near bed (0.05 m) wind speeds recorded during this event were higher (8 m s^{1} compared with 7 m s^{1} for Event 1). The line of *Scaevola* shrubs bordering Site 2 sheltered the more inland instruments during this event (Figure 6). Wenglor B1, situated in the lee of *Scaevola* shrubs, recorded virtually no sedimentation. Significant quantities of sand (3.48 – 32.87 g) collected in the three exposed sand traps, west of the line of *Scaevola* shrubs, during the 20 minute deployment. In contrast, traps in the lee of *Scaevola* collected virtually no sand (Figure 6). The average sand flux downwind of the beach scarp was 35,848.13 g / hour / m^2, but only 295.86 g / hour / m^2 in the lee of the *Scaevola* (between 1300 and 1320 hours and assuming a constant rate of sedimentation). These are significant flux rates given the environmental setting, and they demonstrate the potential for winds crossing the sand cay to transport sand onshore.

4.5 Flow structure over the beach scarp

The two wind events described were distinctive periods of speed-up during an 8-day period of low to moderate speed incident winds. We hypothesize that the differences in the rates of sedimentation measured during the two events are related to the upwind topography – specifically flow acceleration over the beach scarp along much of the north coast of Maaodegalaa (Figure 3). This scarp was present throughout the 8-day deployment but was actively scarped during spring high tides from the 31st January to the 2nd February 2018. Wind velocity contours, derived from the CFD analysis, for the first 10 m above the island, are shown in Figure 17. Accelerated flow over the scarp is characterised by a low velocity zone at the toe of the scarp and high velocity zone after the scarp. The model suggests that this high speed

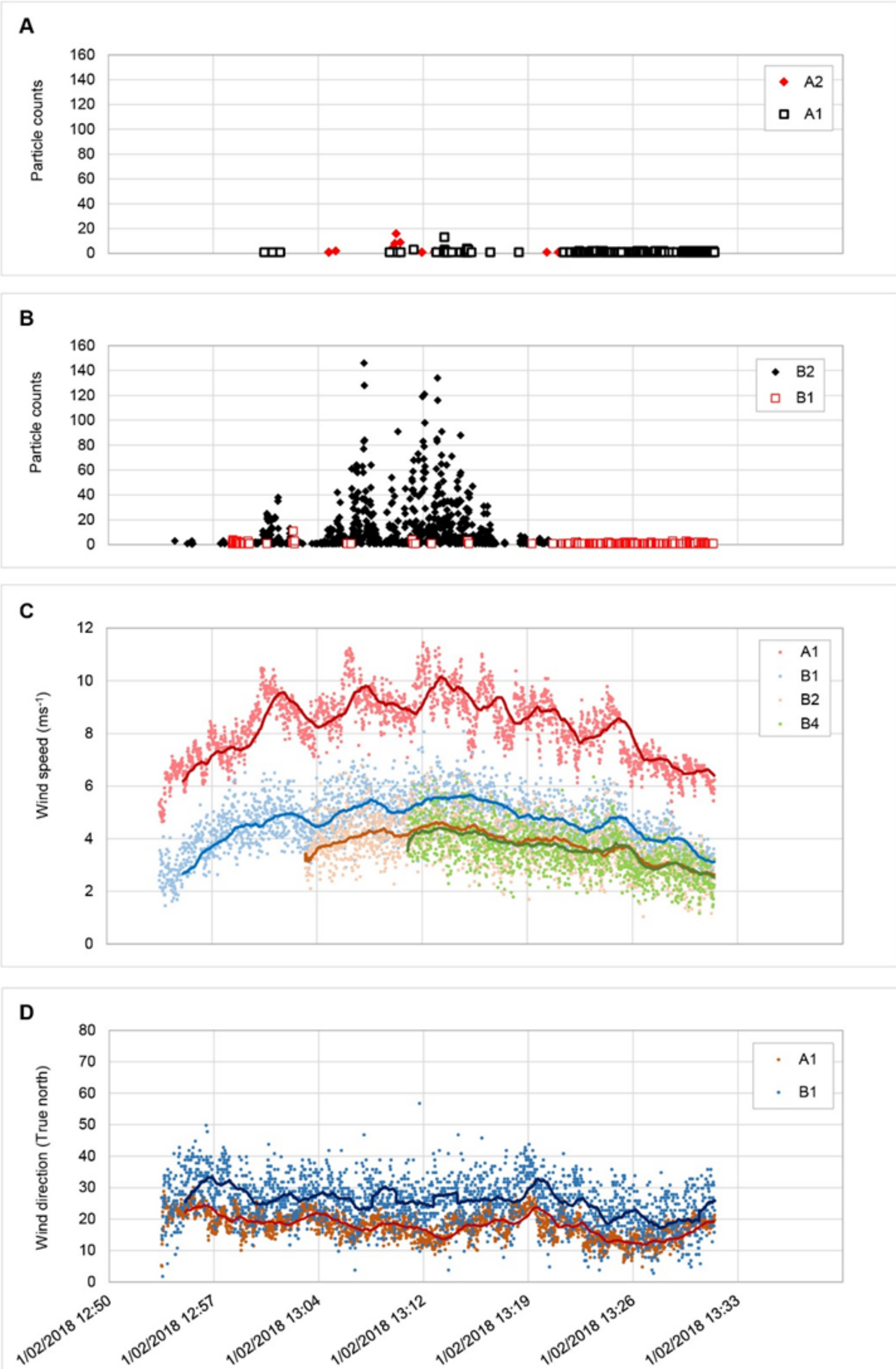

Figure 16: Wenglor particle counts at sites (A) A1 / A2 and (B) B1 / B2; (C) wind speed (A1, 5.53 m and B1-B4, 0.05 m); and (D) wind direction (A1, B1, B2, B4) during Event 2 (1254 - 1332 hours,1st February 2018).

region extends in the direction of flow and moves away from the island surface, in a jet-like structure (as reported by Piscioneri et al. 20190. These structures are seen over larger dunes

(Hesp et al. 2009; Hesp and Smyth 2016) and although the vertical scale here is much smaller the effects are amplified by the abrupt changes in slope at the toe and top of the scarp.

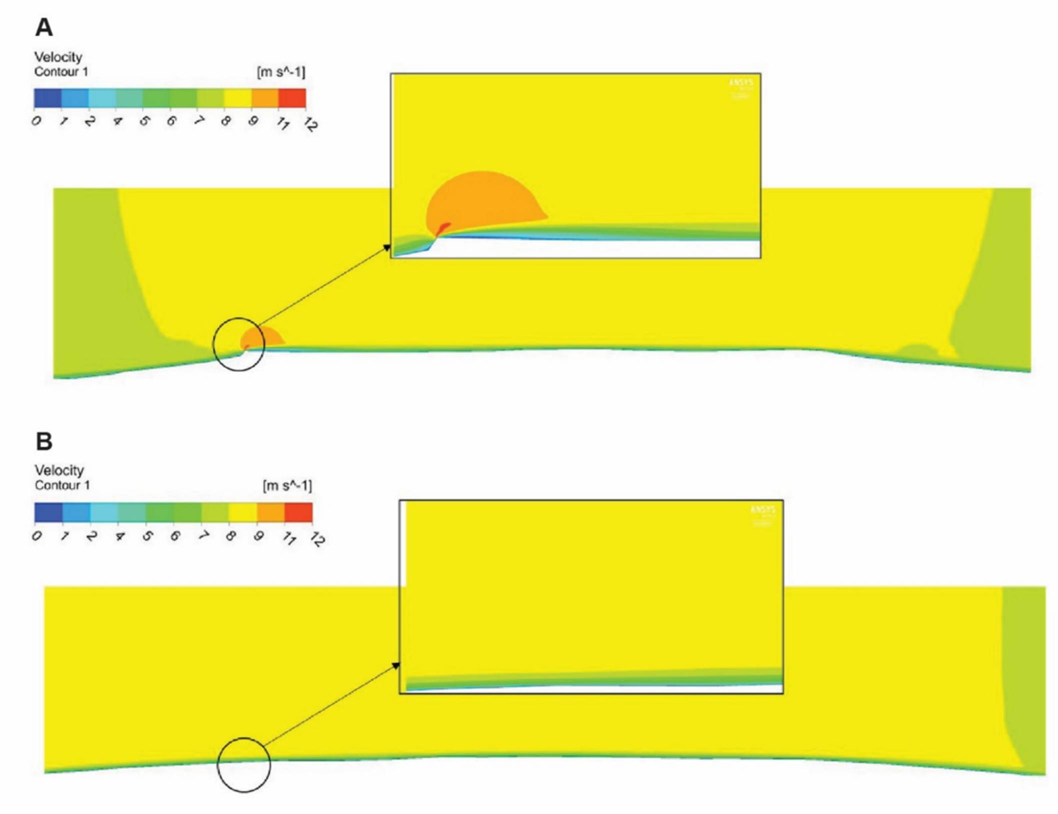

Figure 17: Wind velocity contours for two-dimensional computational fluid dynamics (CFD) simulations across (A) Profile B (scarped) at low tide; and (B) Profile C (un-scarped) at low tide. The simulations show flow acceleration over and downwind of the scarped profile at low tide with an incident wind velocity of 8 m s^{1}.

Derived wind velocity profiles at 1 m from the scarp edge indicate there is a considerable difference between scarped and un-scarped morphologies (Figure18). The influence of the accelerating flow landward of the scarp and the low velocity zone beneath this flow are evident.

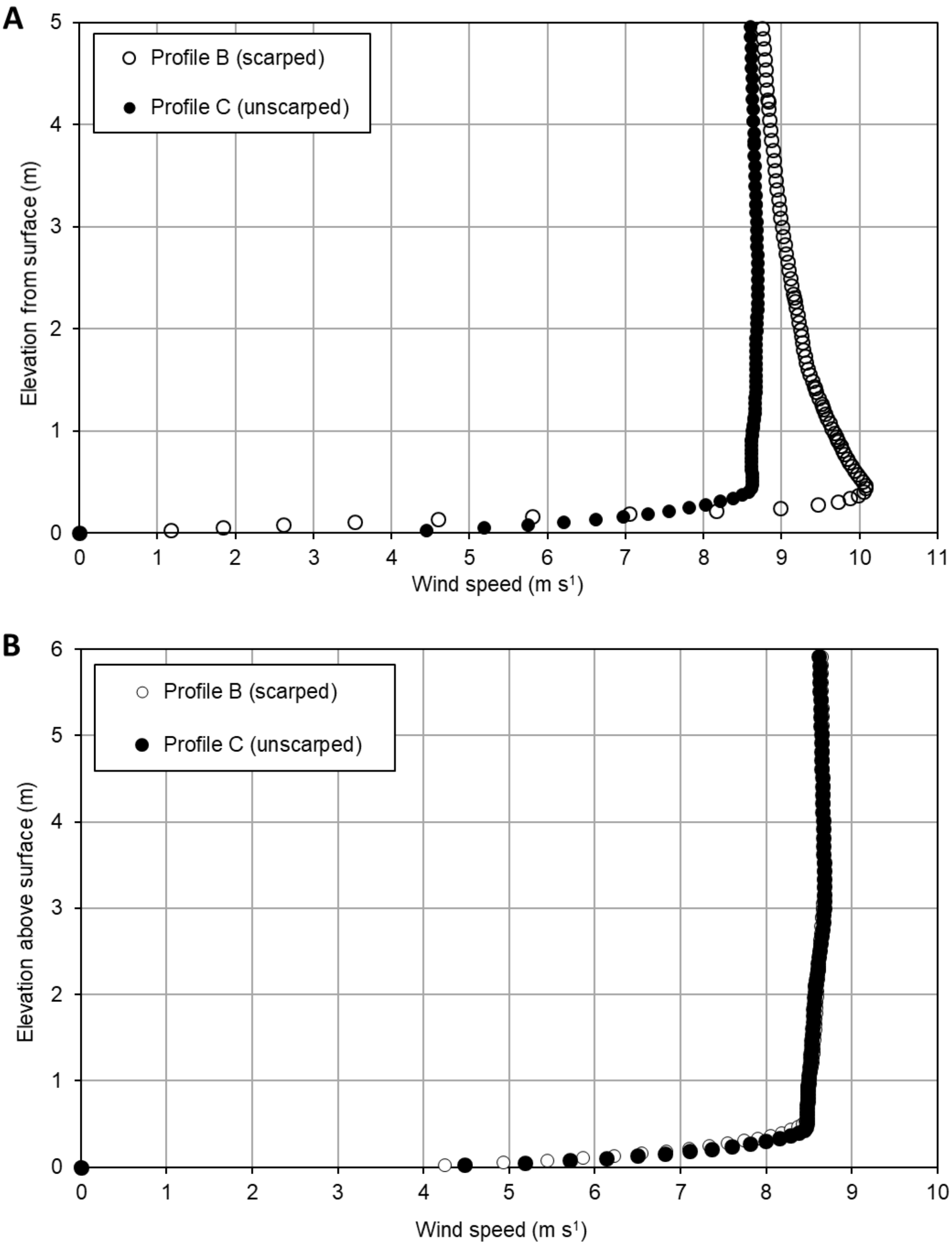

Figure 18: Wind velocity profiles from CFD simulations taken at (A) 1 m and (B) 10 m landward of the scarped and un-scarped beach profiles for an incident wind of 8 m s^{1} crossing the beach at low tide.

The wind velocity for the scarped profile only approaches that of the un-scarped wind velocity profile at elevations above 5 m (Figure 18a). At 10 m landward of the scarp, the wind velocity for the scarped profile reduces to that of the un-scarped profile (Figure 18b). For profile C (un-scarped) the gentle slope of the island means there is only a small increase in wind velocity across the beach, but no speed-up jet over the surface, with a consistent wind velocity profile at 1 m and 10 m, until the flow crosses the south coast (Figure 18b).

5.0 DISCUSSION

The current paper presents the first high-frequency observations of wind flow and aeolian sedimentation in the Maldives during the Iruvai Monsoon. In general, these winds did not generate near-bed flows of sufficient speed to transport sand. However, the experimental period was punctuated by two high wind speed events that generated near-bed speeds in excess of the sediment threshold and we measured saltation and observed the formation of aeolian ripples and shadow dune forms. We hypothesize sand transport by wind was higher during Event 2 because of flow acceleration over adjacent ephemeral beach scarps. CFD analysis supports this interpretation by indicating significant acceleration over the surveyed scarp. Such scarps are a common feature of beaches (Sherman & Nordstrom, 1985) and widely reported in atoll settings (e.g. Rankey, 2011). On Maaodegalaa, they appear to form or be refreshed on the windward side of the island at spring high tide. Scarp formation, therefore, is almost certainly seasonal, with scarps forming on the southern and western margins of the island during the Hulhangu and on the northern side during the Iruvai. Scarping may allow sediment to be eroded and transported towards the core of the island during either monsoon, even when incident winds are below 8m s^{1} at the bed. In this way there is a fortuitous coincidence of onshore incident wind, local wave development and scarp formation during spring high tides during each of the monsoons. It follows that there must be significant periods when these conditions are not met, and aeolian sedimentation as saltation does not occur.

Surface-based density currents under cumulonimbus clouds probably generated the near-surface flows that initiated the measured aeolian sedimentation during the two events described. This phenomenon has not previously been associated with aeolian sand transport in an atoll environment, but is well documented in continental settings (e.g. Wilson et al. 1984). The record of high-frequency wind flow data is brief (only 8 days), and further work is required to determine the magnitude-frequency characteristics of these flows. It may be that the frequency of cumulonimbus cloud formation is more important than seasonal shifts in wind direction and speed associated with the Iruvai and Hulhangu, given ambient wind speeds during both monsoons may be below the critical sand transport threshold. In this regard statistical representations of the annual wind regime, as a wind rose, for example (Figure 2), for example, may misrepresent the relative importance of the Hulhangu and Iruvai monsoons if cumulonimbus cloud formation is critical to aeolian sedimentation. Further observations are necessary to explore the frequency of surface-based density currents and a weather station was installed on Maaodegalaa sand cay in February 2019 to examine this process.

The occurrence of aeolian sedimentation on Maaodegalaa sand cay raises the question of the role this process plays in the formation of islands. Established and densely vegetated islands in Huvadhoo Lagoon may well have formed during a period of sea-level fall during the late-Holocene, as described by East et al. (2018); but this process does not account for the recent development of Maaodegalaa and similar emergent cays in Huvadhoo Atoll. The location of a sand cay on a lagoon platform can be explained by wave transformations and sediment transport as described by Gourlay (1988), and Mandlier and Kench (2012). The dynamic nature of sand cays (Flood and Heatwole, 1986) can, likewise, be explained in terms of variations in the wave climate. But how do sand cays emerge under contemporary sea-state conditions? The presence of wrack on Maaodegalaa indicates that wave overwash has contributed sediment (as well as wrack) to the supratidal island, as documented in recent times following periods of exceptional swell in the Indian Ocean and during tsunami (Kench et al. 2006).

Dune formation in association with pioneer plant species provides a mechanism for islands to accrete to an elevation above the usual level of wave swash. We collected 11 plant species during fieldwork and all are early successional species that are marine dispersed (described in Sujanapal & Sankaran, 2016). We observed small nebkha developed around individual plants of *Cyperus conglomeratus* and larger nebkha formed with *Scaevola taccada*. *Cyperus* may be particularly important in explaining patterns of aeolian sedimentation and accretion. It has a tussock-like (or 'bunch-grass') growth form and occurs on Maaodegalaa as scattered plants (see Figure 3). In this respect, it is not unlike pioneer dune species such as *Ammophila arenaria*, except it does not spread by subsurface rhizomes or stolons. Nor does it have the capacity to produce vertical rhizomes and grow vertically as sand accumulates. However, it does appear to encourage sand deposition because of its community structure. Individuals of the species tend to be widely scattered, so that sand may be blown into this community, where it settles as sub-canopy wind speeds decline. We measured accretion of 0.3 m over 13 months within the *Cyperus* community that developed between fieldwork in January 2017 and February 2018 – which is a significant contribution to the topography of the sand cay. However, this process may be time-limited, since aeolian sedimentation and accretion is likely to decline as *Cyperus* increases in density or following the establishment of *Scaevola* within the Cyperus community. We measured low wind speeds in the lee of *Scaevola* during Event 2 on Maaodegalaa, which suggests any period of general aeolian accretion in conjunction with *Cyperus* might be short lived.

We propose a conceptual model of lagoon island formation, with both overwash and aeolian sedimentation contributing to island accretion. Island emergence depends on the favourable coincidence of tidal and wind conditions and the presence of viable plant seed and favourable germination conditions (e.g. rainfall and soil moisture). The initial condition is a sand cay formed as wave processes transport sediment to a nodal depocentre on the reef surface (Figure 19a). Sand cays near to Maaodegalaa in this condition are over-washed at spring high tide, but at certain times of the year they may emerge for periods during a sequence of successively lower spring high tides. During this period, if growth conditions are favourable, stranded seeds may germinate and grow on the exposed substrate. Seedlings or maturing plants may then intercept sand blown across the newly exposed sand cay surface (Figure 19b). Sand may also be trapped around and in the lee of wrack, providing an additional depth of sand for root development. This process may continue so long as spring high tides in the rising phase of the annual tidal cycle do not inundate the island (and wave overwash events do not occur). We examined the tidal records for Gan for 2015 and 2016, located 105 km to the south of Maaodegalaa. The difference in elevation between the highest and lowest spring high tides during 2015 was 0.35 m. The maximum elevation of the highest spring tide was 2.42 m on the 27th October 2015. Subsequent spring tides did not reach this level during all of 2016, when the maximum spring high tide reached 2.32 m. Sand cay accretion may then continue as a result of aeolian activity and the deposition of sediment resulting from wave over-wash (Figure 19c).

Aeolian activity is enhanced, we hypothesize, by flow acceleration over beach scarps eroded during spring high tides. The highest high tides may inundate the lower island surfaces, and the sand cay will remain vulnerable to tsunami (as occurred in 2004; Kench et al. 2006), however, at this stage the sand cay has accreted above the reach of swash and plant colonisation and growth can continue. There is a useful coincidence of beach scarping and incident wave direction during the seasonal monsoons, such that there is no true windward or leeward side to a sand cay on an annual basis. Sand can be transported toward the core of the sand cay during either monsoon. At this stage, the development of a stable island form is not inevitable. Seasonal variations in wave characteristics might result in the total erosion of the island and the re-establishment of a subtidal sand cay elsewhere on the reef platform. The current sand cay of Maaodegalaa developed from a cay which was situated to the northwest of its current location. Sand cays such as Maaodegalaa may transition through multiple forms and locations before they develop into more stable island forms.

The emergence of a sand cay above the limit of tides and their colonisation by pioneer plant species is commonly described as a sequence of events (e.g. Hopley & Heatwole, 2011),

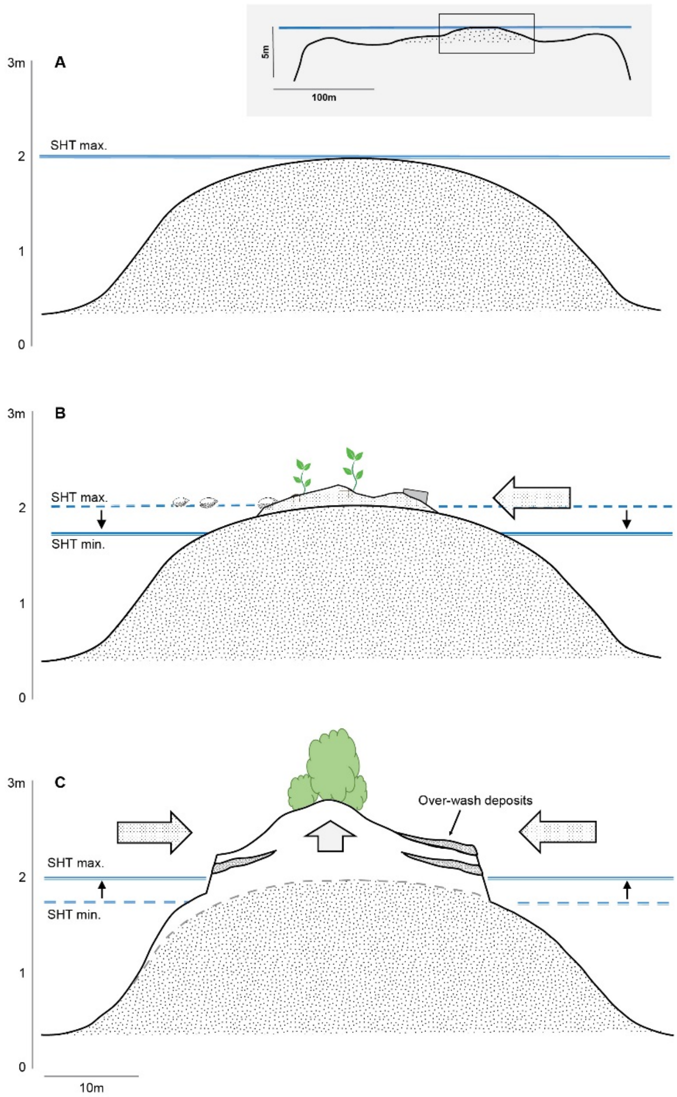

Figure 19: Conceptual model of sand cay emergence and accretion. The sand cay forms on the reef platform and is over-washed by waves at the highest spring high tides (A). Subsequent (lower) spring tides strand wrack and seed on the cay, and expose the cay surface (B). Seeds germinate, reptation and saltation builds nebkha, and shadow dunes form around wrack and plants. The cay accretes above the level of the highest spring tides aided, in part, by flow acceleration over seasonal high-tide beach scarps (C). Occasional over-wash during periods of high wave activity / tsunami (labelled) contribute to island accretion. Aeolian sedimentation and accretion becomes localised as shrub cover increases.

where a barren sand surface is colonised by pioneer plant species. The above model envisages island emergence by aeolian sedimentation and plant colonisation are coincident – the initial supratidal bed provides a surface for marine-dispersed seeds to germinate, and the roughness created by subsequent plant growth provides for sand accumulation and nebkha development. Significantly, this new model of contemporary island development is independent of sea-level over short (decadal) time scales, which is known to be rising in the Maldives at a rate of 0.8 – 1.6 mm y^{1} (Church et al. 2004; Woodworth, 2005).

6.0 CONCLUSIONS

Aeolian sand transport of fine to medium, well-sorted, coral sands was recorded on Maaodegalaa sand cay during two wind events. This is the first high-frequency measurement of this process in the Maldives and in an equatorial lagoon island setting. It is likely this process occurs frequently and in a range of geomorphic settings in Huvadhoo Atoll and in other atolls, including low sand terraces on established islands. Reptation and aeolian ripple development probably occurs frequently when near-surface flows exceed 6 m s^{1}. Saltation occurs at higher wind speeds, but probably in very specific geomorphic circumstances. We recorded much higher rates of sand transport as saltation downwind of a beach scarp due to flow acceleration. Incident winds associated with the Iruvai monsoon may not be able to initiate sand transport, but we recorded near-surface winds in excess of 8 m s^{1}, probably generated by surface-based density currents under cumulonimbus clouds.

The rates of sand transport measured are not high, but are significant in the context of a low-lying coral sand cay with a maximum elevation 0.9 m above the level of the highest spring high tides and 0.6 m above the limit of wave swash. Island accretion by aeolian sedimentation and dune development may account for a significant component of the island topography, however, wave-forced over-wash and sand deposition must also contribute. Indeed, such events may be critical to island development since they deliver the seeds of terrestrial plant species to an elevation above the usual reach of tides. Subsequent plant colonisation and growth is critical to nebkha development.

Our results provide the first observations of aeolian processes facilitating island accretion beyond the limits of wave run-up and overwash. Such a mechanism, combined with colonisation by vegetation, may be critical in the transformation of cays from dynamic ephemeral features on reef surfaces to more stable and fully vegetated islands. Of note, the Maaodegalaa case study demonstrates that small islands may form under contemporary conditions of rising sea-level. Is there a phase of aeolian activity in the development of all lagoon islands? This should be possible to confirm, if such activity is associated with the formation of a distinct aeolian facies, by sampling the stratigraphy of well-established islands.

7.0 ACKNOWLEDGEMENTS

[redacted]

8.0 REFERENCES

Ardon, K., Tsoar, H., Blumberg, D.G., 2009. Dynamics of nebkhas superimposed on a parabolic dune and their effect on the dune dynamics. J. Arid Environ. 73, 1014 – 1022.

Mohamed Aslam, Kench, P.S., 2017. Reef island dynamics and mechanisms of change in Huvadhoo Atoll, Republic of Maldives, Indian Ocean. Anthropocene 18, 57–68.

Bauer, B., Davidson-Arnott, R., Hilton, M.J., Fraser, D., 2018. On the frequency response of a Wenglor particle-counting system for aeolian transport measurements. Aeol. Res. 32, 133-140.

Bayne, C.J., Cogan, B.H., Diamond, A.W., Frazier, J., Grubb, P., Hutson, A., Poore, M.E.D., Stoddart, D.R., Taylor, J.D., 1970. Geography and Ecology of Cosmoledo Atoll. Atoll Res. Bull. 136, 37-56.

Church, J.A., White, N.J., Coleman, R., Lambeck, K., Mitrovica, J.X., 2004. Estimates of the regional distribution of sea-level rise over the 1950–2000 period. J. Climate 17, 2609–2625.

Durrant, T., Greenslade, D., Hemer, M., Trenham, C., 2014. A global wave hindcast focussed on the Central and South Pacific. CAWCR Technical Report No. 070, Bureau of Meteorology, Government of Australia, 54pp.

East, H.K., Perry, C.T., Kench, P.S., Liang, Y., Gulliver, P., 2018. Coral Reef Island Initiation and Development Under Higher Than Present Sea Levels. Geophys. Res. Letts. 45. https://doi.org/10.1029/2018GL079589.

Feng, Z., Hagos, S., Rowe, A.K., Burleyson, C.D., Martini, M.N., de Szoeke, S.P., 2015. Mechanisms of convective cloud organization by cold pools over the tropical warm ocean during the AMIE/DYNAMO field campaign. J. Adv. Model. Earth Syst. 7, 357–381.

Flood, P.G., Heatwole, H., 1986. Coral cay instability and species-turnover of plants at Swain Reefs, southern Great Barrier Reef, Australia. J. Coast. Res. 2, 479–496.

Gourlay, M.R., 1988. Coral cays: products of wave action and geological processes in a biogenic environment. Proceedings Sixth International Coral Reef Symposium, Townsville, 2, 491-496.

Harangozo, S.A., 1992. Flooding in the Maldives and its implications for the global sea-level rise debate. Sea Level Changes: Determination and Effects. Geophys. Mono. 69. IUGG, 11, 95–100.

Hesp, P.A., 2008. Coastal Dunes in the Tropics and Temperate Regions: Location, Formation, Morphology and Vegetation Processes, in: Martínez, M.L., Psuty N.P. (Eds.), Ecological Studies, Vol. 171. Coastal Dunes, Ecology and Conservation © Springer-Verlag, Berlin pp. 22-49.

Hesp, P.A., Walker, I.J., Davidson-Arnott, R., Bauer, B.O., Ollerhead, J., 2009. Storm wind flow over a foredune, Prince Edward Island, Canada. J. Coastal Res. SI 56, 312-316.

Hesp, P.A., Smyth, T.A., 2016. Jet flow over foredunes. Earth Surf. Proc. Land. 41, 1727-1735.

Hilton, M.J., Nickling, B., Wakes, S., Sherman, D., Konlechner, T., Jermy, M., Geoghegan, P., 2017. An efficient, self-orienting, vertical-array, sand trap. Aeol. Res. 25, 11-21.

Hopley, D., Heatwole, H., 2011. Vegetated Cays, in: Hopley D. (Ed.) Encyclopedia of Modern Coral Reefs: Structure Form and Process, Springer, The Netherlands, p. 648-653.

Houze, R.A., Jr., 2004. Cloud Dynamics, Elsevier Science & Technology, Oxford. pp.496.

Houze, R. A. Jr., 2004. Mesoscale convective systems. Rev. Geophys. 42, https://doi.org/10.1029/2004RG000150.

Kench, P.S., 2011. Maldives, in: Hopley D. (Ed.) Encyclopedia of Modern Coral Reefs: Structure Form and Process, Springer, The Netherlands, p. 1138-1139.

Kench, P.S., McLean, R.F., Nichol, S.L., 2005. New model of reef-island evolution: Maldives, Indian Ocean. Geology 33, 145-148.

Kench, P.S., Brander, R.W., 2006. Response of reef island shorelines to seasonal climate oscillations: South Maalhosmadulu Atoll, Maldives. J. Geophys. Res. 111: doi:10.1029/2005JF000323.

Kench, P.S., McLean, R.F., Brander, R.W., Nichol, S.L., Smithers, S.G., Ford, M.R., Parnell, K.E., Mohammed Aslam, 2006. Geological effects of tsunami on mid-ocean atoll islands: The Maldives before and after the Sumatran tsunami. Geology 34, 177-180.

Kench, P.S., Brander, R.W., Parnell, K.E., McLean, R.F., 2006. Wave energy gradients across a Maldivian atoll: Implications for island geomorphology. Geomorphology 81, 1–17.

Kench, P.S., Nichol, S., Mclean, R.F., Smithers, S.G., Brander, R.W., 2007. Impact of the Sumatran Tsunami on the geomorphology and sediments of reef islands: South Maalhosmadulu Atoll, Maldives. Atoll Res. Bull. 544, pp. 105-134.

Liang, Y., Kench, P.S., Ford, M.R., East, H.K., 2016. Lagoonal reef sediment supply and island connectivity, Huvadhoo Atoll, Maldives. J. Coast. Res. Special Issue 75 - Proceedings of the 14th International Coastal Symposium, Sydney, 6-11 March 2016: pp. 587 – 591.

Mandlier, P.G., Kench, P.S., 2012. Analytical modeling of wave refraction and convergence on coral reef platforms: implications for island formation and stability. Geomorphology 159-160, 84-92.

Marriner, N., Guérout M., Romon, T., 2010. The forgotten slaves of Tromelin (Indian Ocean): new geoarchaeological data. J. Archaeol. Sci. 37, 1293–1304.

McKoy, H., Kennedy, D.M., Kench, P.S., 2010. Sand cay evolution on reef platforms, Mamanuca Islands, Fiji. Mar. Geol. 269, 61 - 73.

Perianez R., 2004. A particle-tracking model for simulating pollutant dispersion in the Strait of Gibralter. Mar. Pollut. Bull. 49, 613-623.

Perry, C.T., Edinger, E.N., Kench, P.S., Mumby, P.J., Murphy, G., Steneck, R.S., Smithers, S.G., 2012. Estimating rates of biologically driven coral reef framework production and erosion: A new census-based carbonate budget methodology and applications to the reefs of Bonaire. Coral Reefs 31, 853–868.

Perry, C.T., Kench, P.S., O'Leary, M.J., Morgan, K.M., Januchowski-Hartley, F., 2015. Linking reef ecology to island building: Parrotfish identified as major producers of island-building sediment in the Maldives. Geology 43, 503–506.

Perry, C.T., Kench, P.S., Smithers, S.G., O'Leary, M., Yamano, H., McGuirk, P., 2013. Timescales and Modes of Faro Infill: Constraining Thresholds of Reef Island Formation. Geology 41, 1111-1114.

Piscioneri, N., Smyth, T.A.G., Hesp, P.A. (2019) Flow dynamics over a foredune scarp. Earth Surf. Proc. Land. https://doi.org/10.1002/esp.4555.

Rankey, E.C., 2011. Nature and stability of atoll island shorelines: Gilbert Island chain, Kiribati, equatorial Pacific. Sedimentology 58, 1831-1859.

Sherman, D., Nordstrom, K., 1985. Beach scarps. Z. Geomorphol. 29, 139-152.

Stoddart, D.R., Taylor, J.D., 1971. Geography and Ecology of Diego Garcia Atoll, Chagos Archipelago. Atoll Res. Bull. No. 149. The Smithsonian Institute, Washington D.C. 237pp.

Storz, D., Gischler, E., 2011. Coral extension rates in the NW Indian Ocean II: reconstruction of 20th century Indian monsoon strength and rainfall over India. Geo-Mar. Lett. 31, 155 – 162.

Schotte, F.A., McCreary Jr., J.P., 2001. The monsoon circulation of the Indian Ocean. Prog. Oceanogr. 51, 1–123.

Sujanapal, P., Sankaran, K.V., 2016. Common Plants of the Maldives. Food and Agriculture Organization of the United Nations, Bangkok, 301pp.

Wadey, M., Brown, S., Nicholls, R.J., Haigh, I., 2017. Coastal flooding in the Maldives: an assessment of historic events and their implications. Nat. Hazards 89, 131–159.

Wakes, S.J., Maegli, T., Dickinson, K.J.M., 2010. Numerical modelling of wind flow over a complex geometry. Environ. Modell. Softw. 25, 237-247.

Wilson, J. W., Roberts, R.D., Kessinger, C., McCarthy, J., 1984. Microburst wind structure and evaluation of Doppler radar for airport wind shear detection. J. Climate Appl. Meteor. 23, 898–915.

Woodroffe, C.D., 2008. Reef-island topography and the vulnerability of atolls to sea-level rise. Global Planet. Change 62, 77–96.

Woodroffe, C.D., McLean, R.F., 1994. Reef Islands of the Cocos (Keeling) Islands. Atoll Res. Bull. 409. The Smithsonian Institute, Washington D.C. 36pp.

Woodworth, P.L., 2005. Have there been large recent sea-level changes in the Maldive Islands? Global Planet. Change 49, 1–18.

Supplementary materials

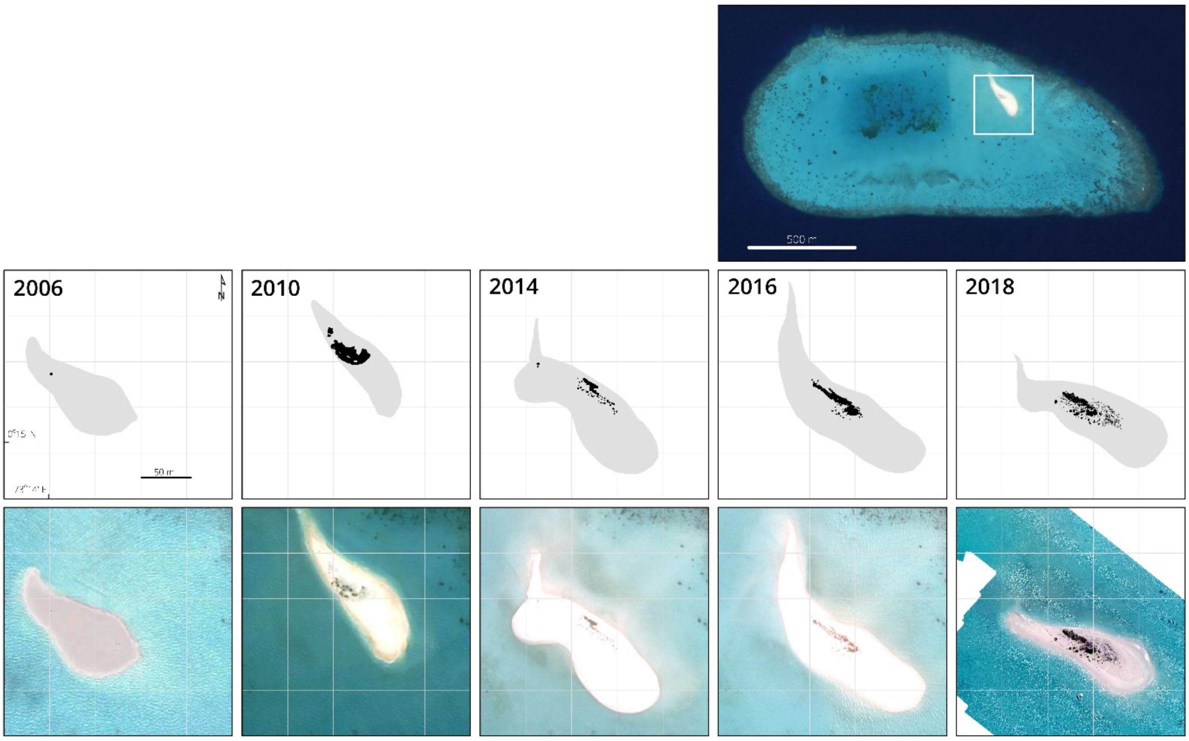

The location of Maaodegalaa on the reef platform and stages in its position and colonisation by vegetation (2006 – 2018).

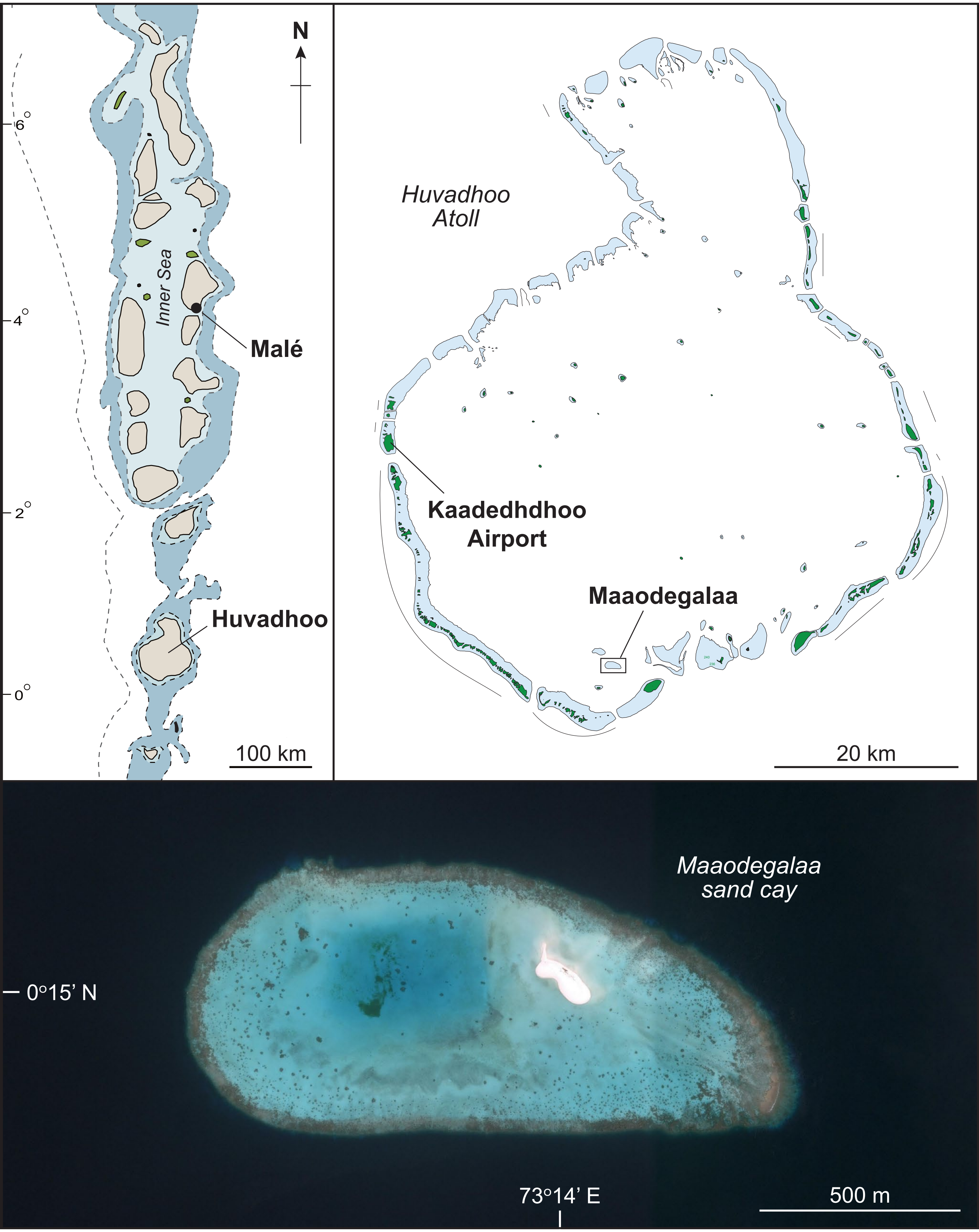
N
6°
4°
2°
0°
Inner Sea
Malé
Huvadhoo
100 km
Huvadhoo
Atoll
Kaadedhdhoo
Airport
Maaodegalaa
20 km
Maaodegalaa
sand cay
0°15' N
73°14' E
500 m

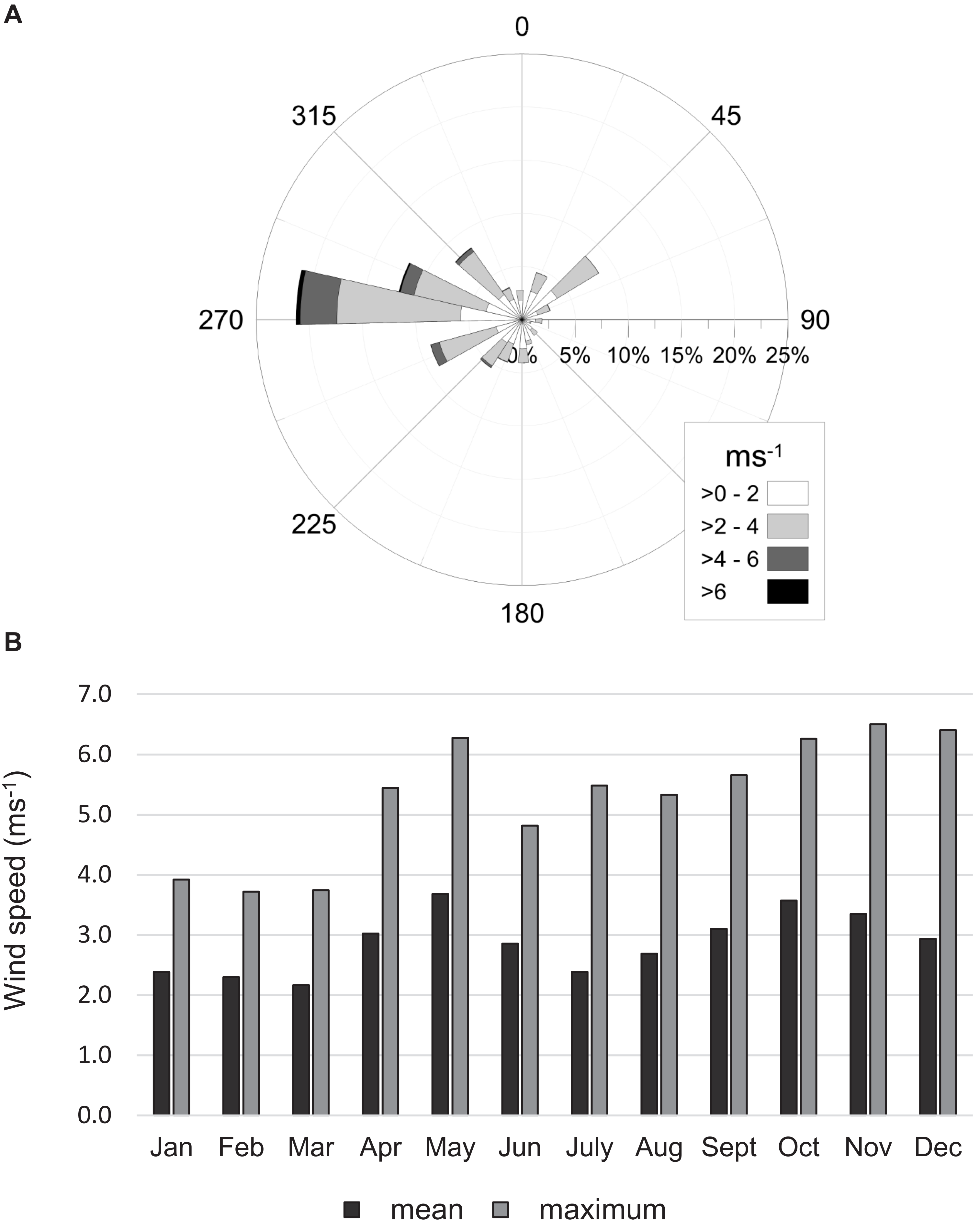

A
0
45
90
180
225
270
315
0%
5%
10%
15%
20%
25%
ms-1
>0 - 2
>2 - 4
>4 - 6
>6
B
Wind speed (ms-1)
7.0
6.0
5.0
4.0
3.0
2.0
1.0
0.0
Jan
Feb
Mar
Apr
May
Jun
July
Aug
Sept
Oct
Nov
Dec
mean
maximum

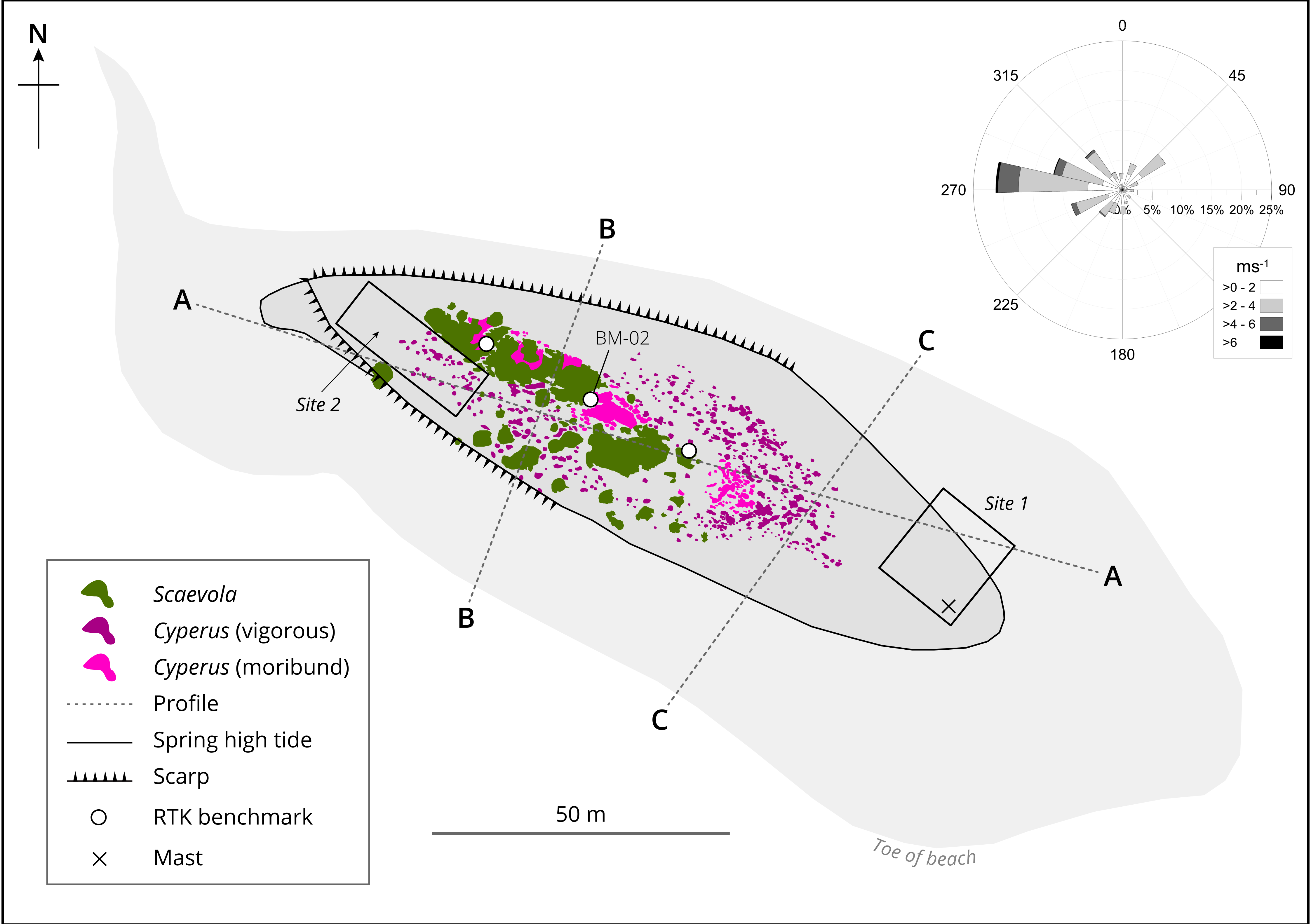
N
A
A
B
B
C
C
Site 1
Site 2
BM-02
Toe of beach
50 m
0
45
90
180
225
270
315
5%
10%
15%
20%
25%
ms-1
>0 - 2
>2 - 4
>4 - 6
>6
Scaevola
Cyperus (vigorous)
Cyperus (moribund)
Profile
Spring high tide
Scarp
RTK benchmark
Mast

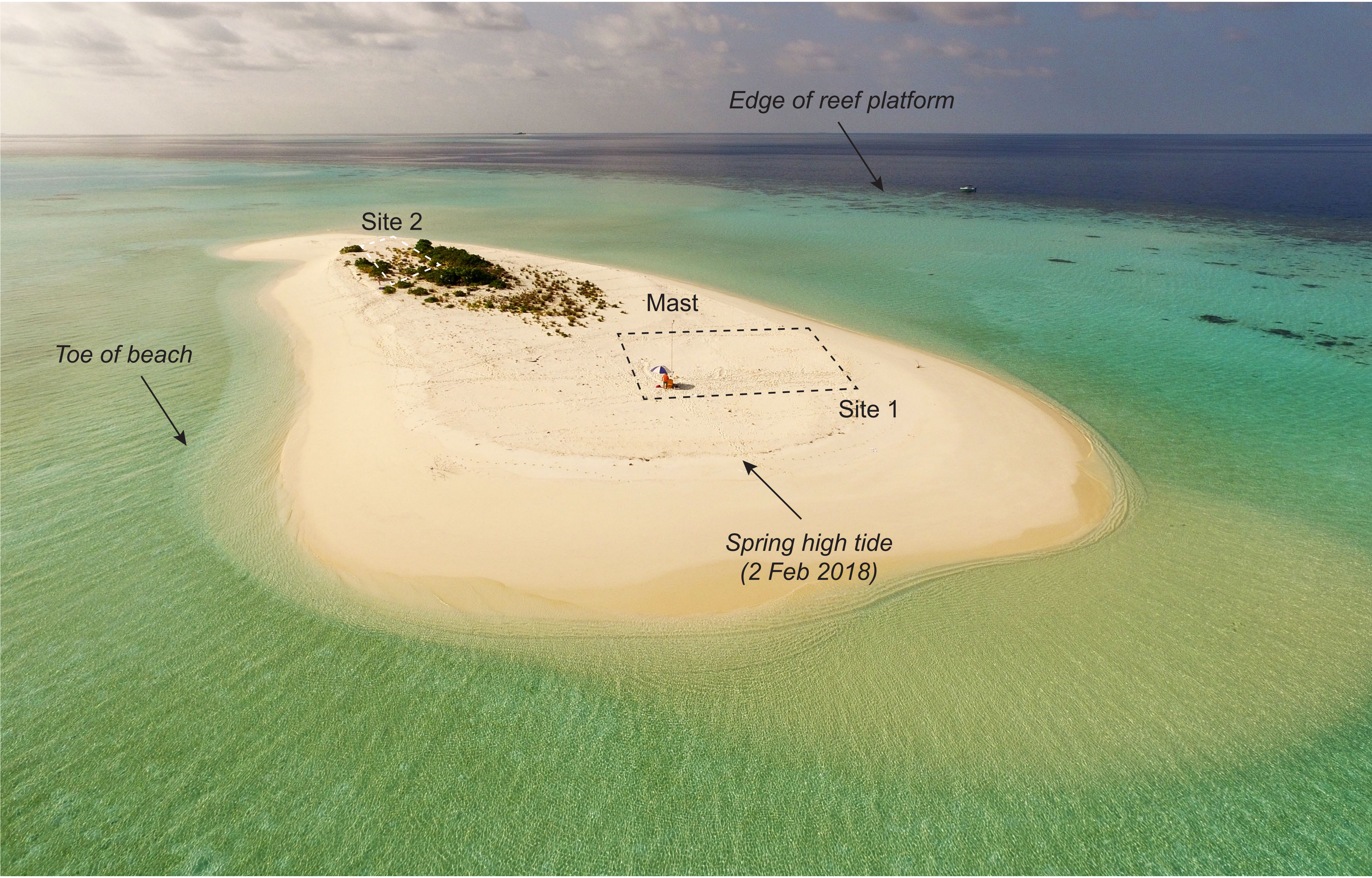
Edge of reef platform
Site 2
Mast
Toe of beach
Site 1
Spring high tide
(2 Feb 2018)

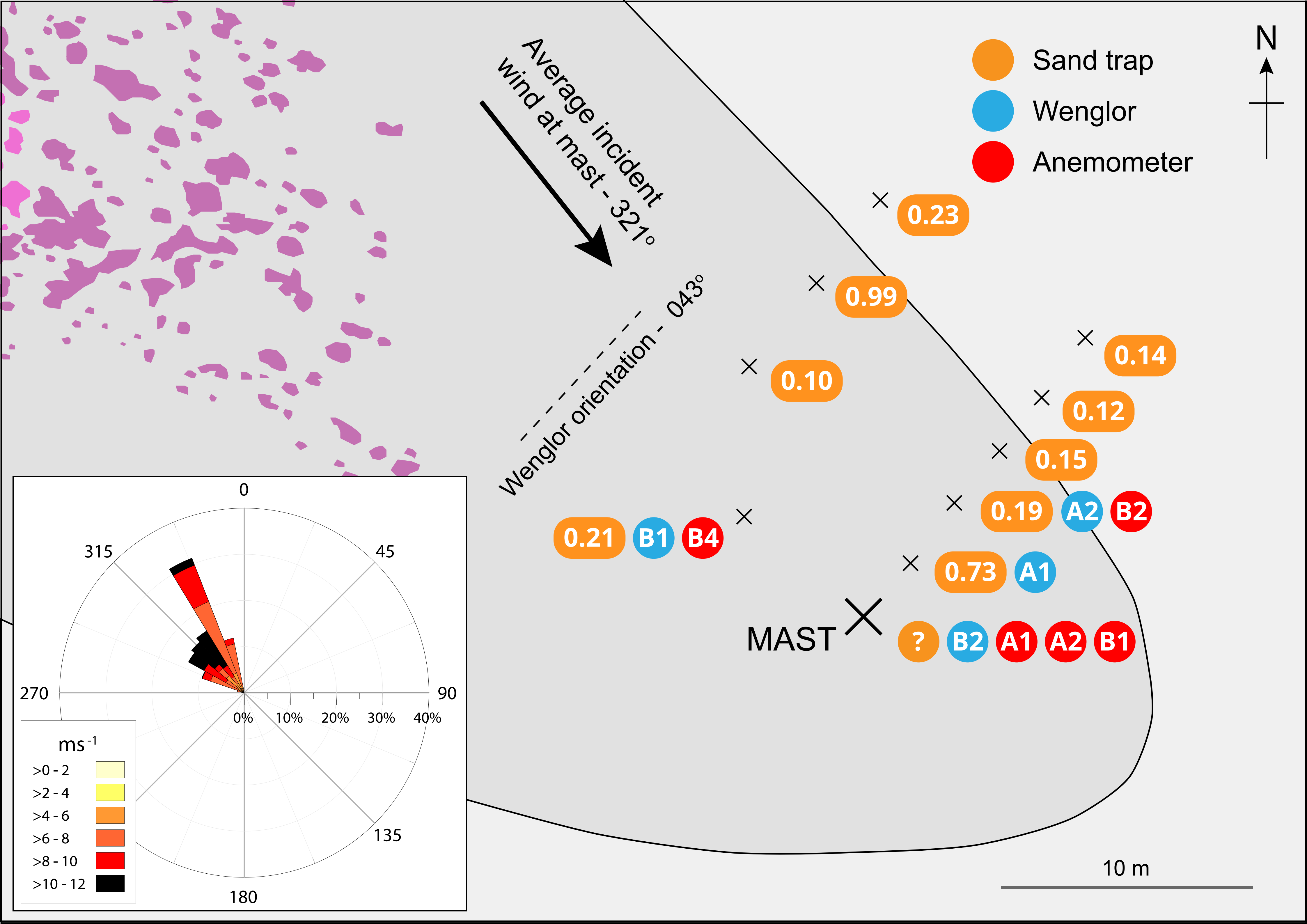
N
Sand trap
Wenglor
Anemometer
Average incident wind at mast - 321°
Wenglor orientation - 043°
0.23
0.99
0.14
0.10
0.12
0.15
0.19
A2
B2
0.21
B1
B4
0.73
A1
MAST
?
B2
A1
A2
B1
10 m
0
45
90
135
180
270
315
0%
10%
20%
30%
40%
ms-1
>0 - 2
>2 - 4
>4 - 6
>6 - 8
>8 - 10
>10 - 12

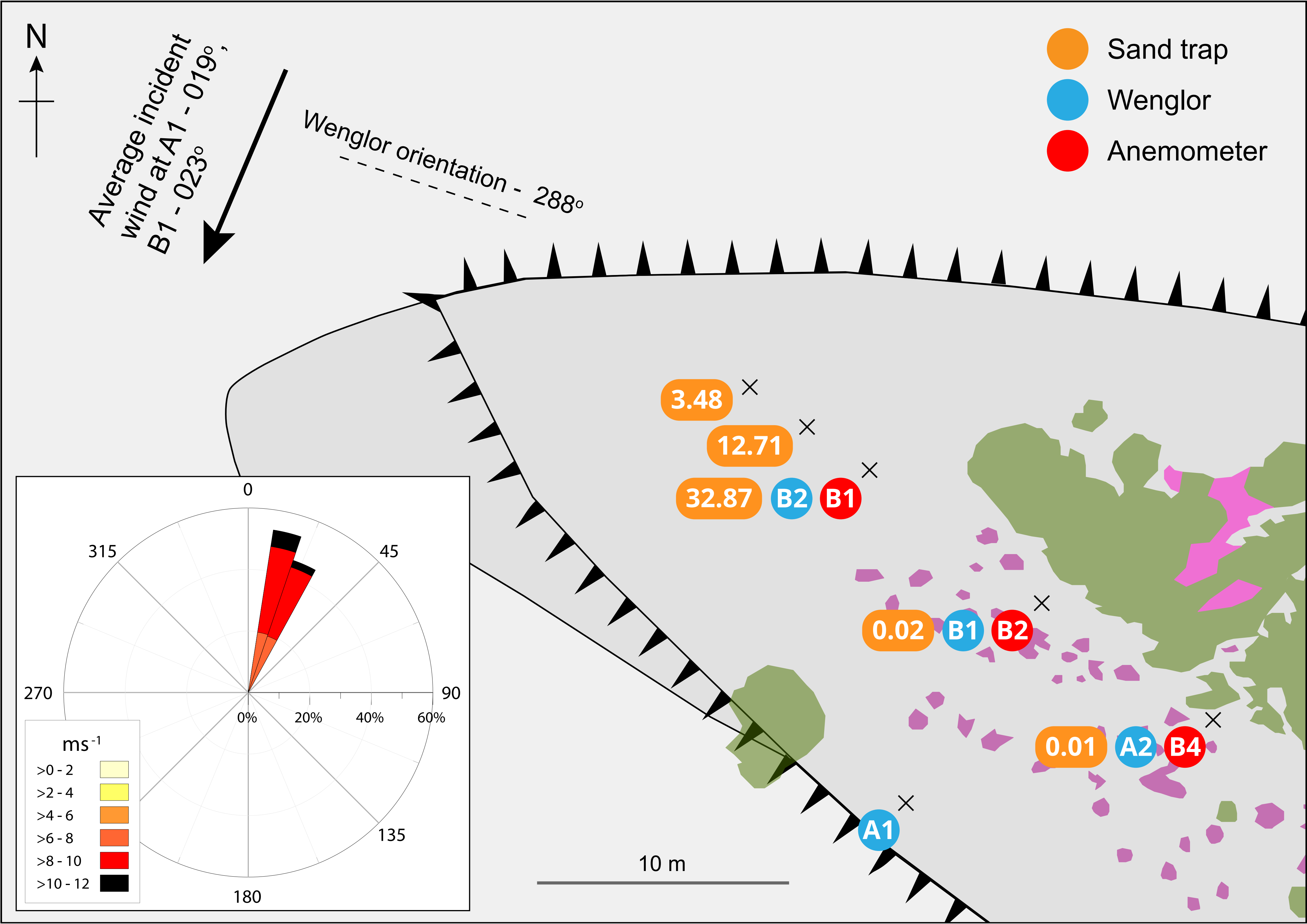
N
Average incident wind at A1 - 019°, B1 - 023°
Wenglor orientation - 288°
Sand trap
Wenglor
Anemometer
3.48
12.71
32.87
B2
B1
0.02
B1
B2
0.01
A2
B4
A1
10 m
0
45
90
135
180
270
315
0%
20%
40%
60%
ms-1
>0 - 2
>2 - 4
>4 - 6
>6 - 8
>8 - 10
>10 - 12

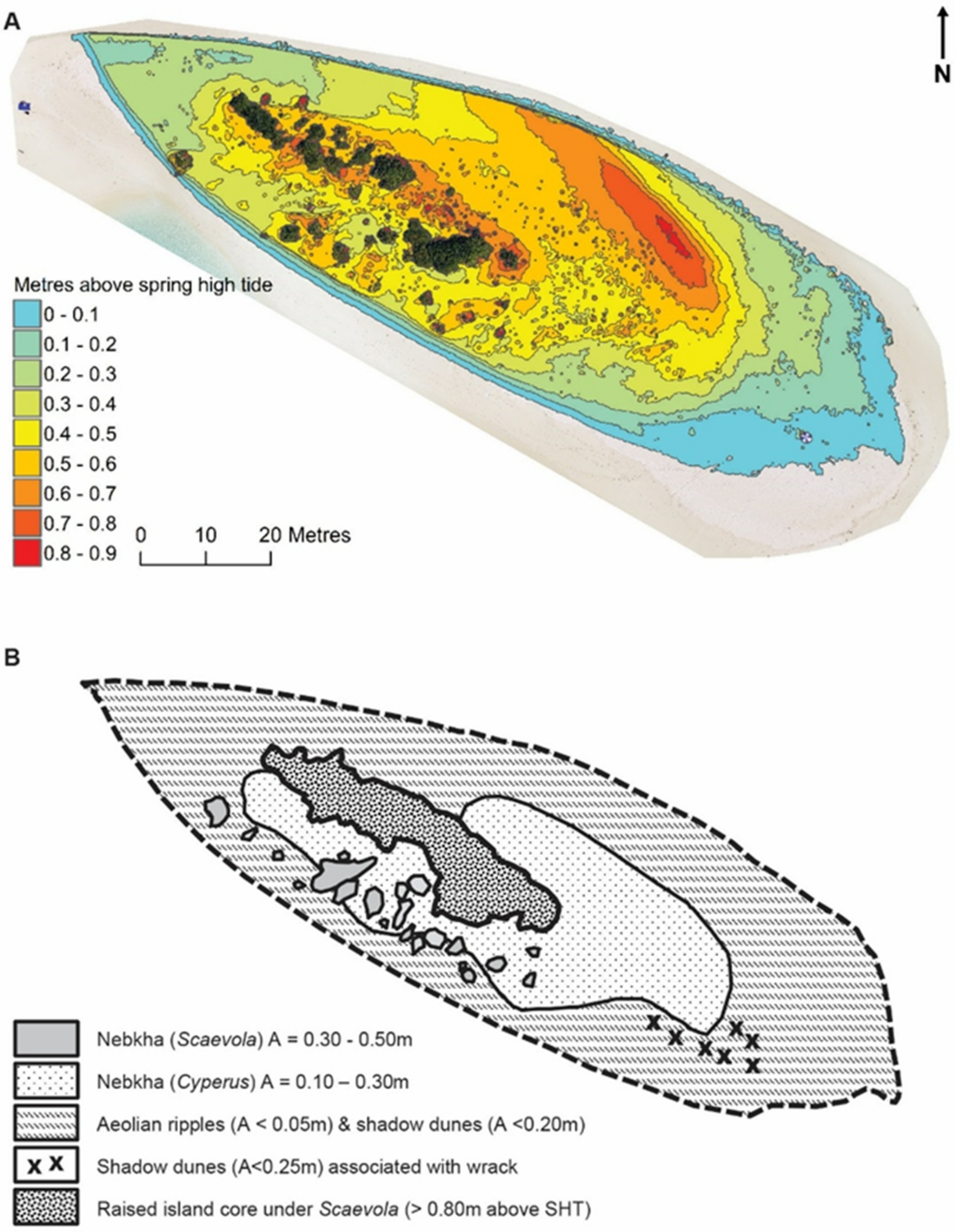
A
N
Metres above spring high tide
0 - 0.1
0.1 - 0.2
0.2 - 0.3
0.3 - 0.4
0.4 - 0.5
0.5 - 0.6
0.6 - 0.7
0.7 - 0.8
0.8 - 0.9
0
10
20 Metres
B
Nebkha (Scaevola) A = 0.30 - 0.50m
Nebkha (Cyperus) A = 0.10 – 0.30m
Aeolian ripples (A < 0.05m) & shadow dunes (A <0.20m)
Shadow dunes (A<0.25m) associated with wrack
Raised island core under Scaevola (> 0.80m above SHT)

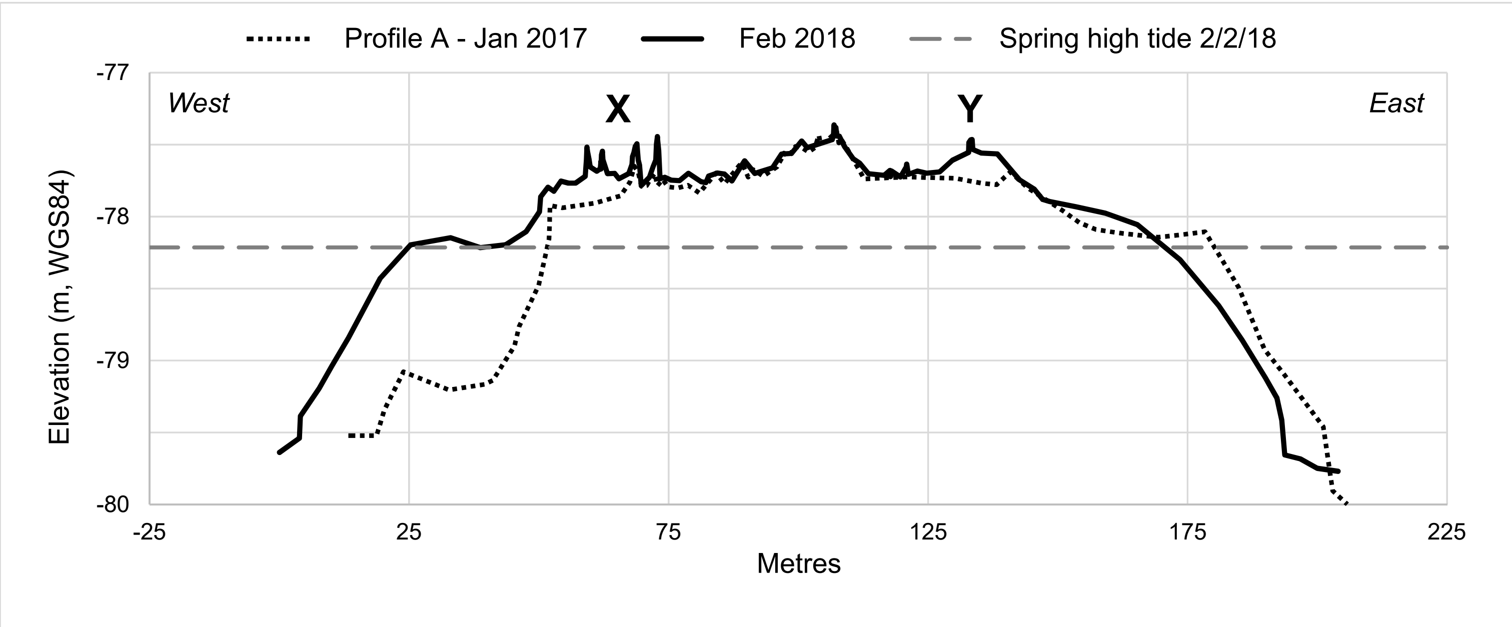
Profile A - Jan 2017
Feb 2018
Spring high tide 2/2/18
West
East
X
Y
Elevation (m, WGS84)
-77
-78
-79
-80
-25
25
75
125
175
225
Metres

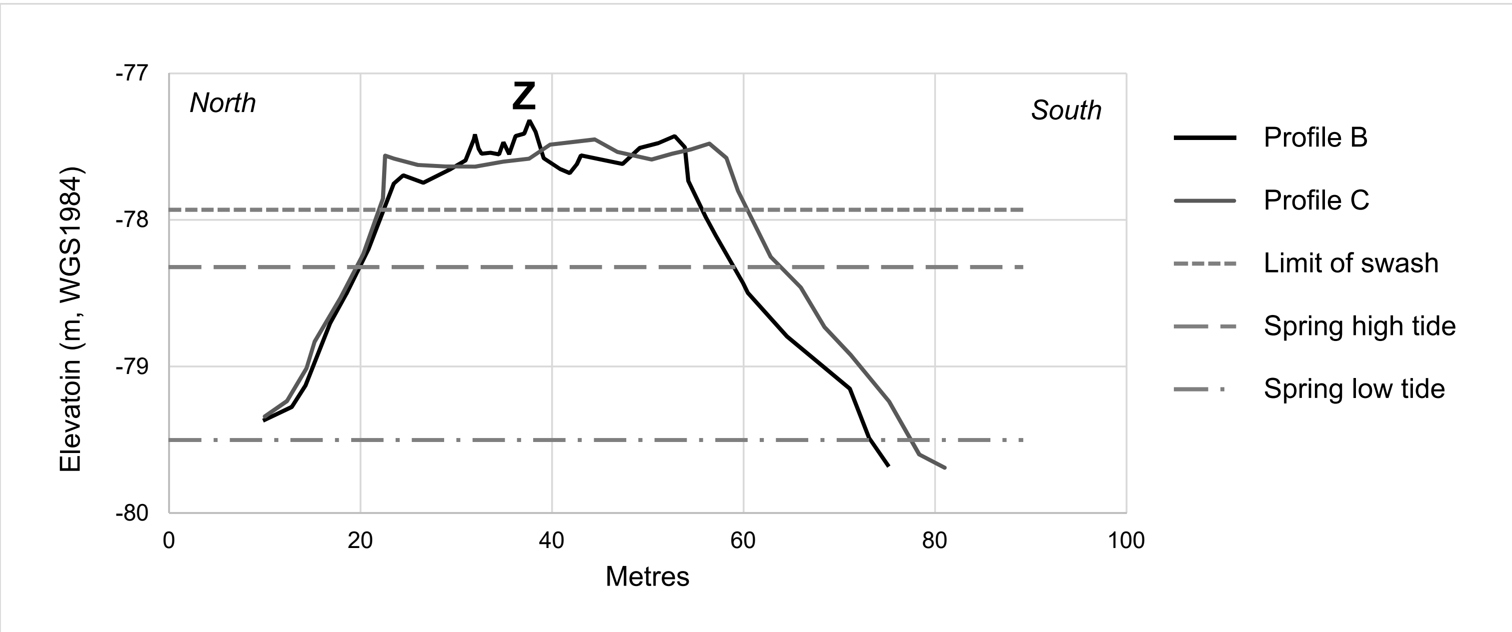
North
South
Z
Elevatoin (m, WGS1984)
-77
-78
-79
-80
0
20
40
60
80
100
Metres
Profile B
Profile C
Limit of swash
Spring high tide
Spring low tide

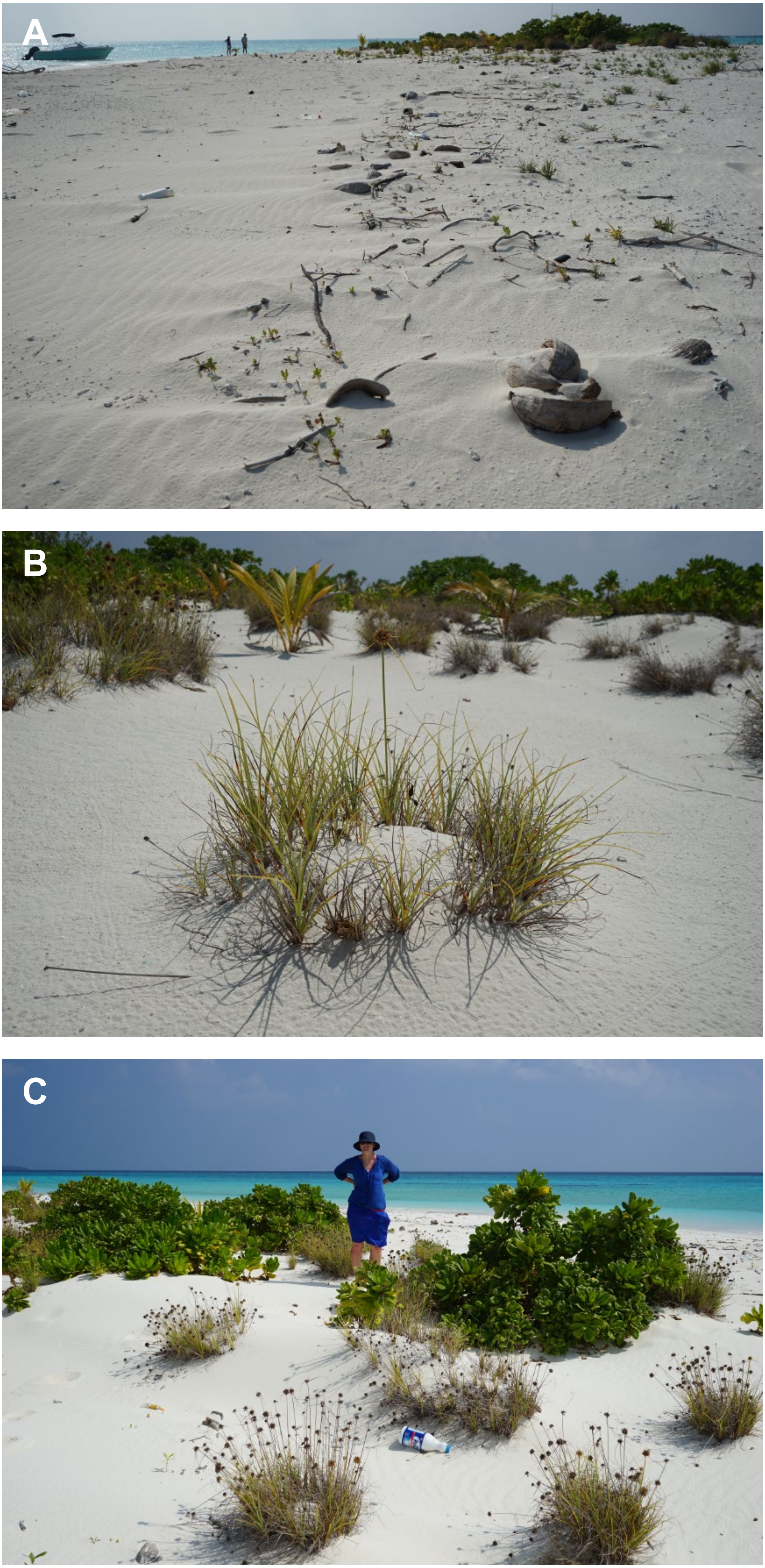
A
B
C

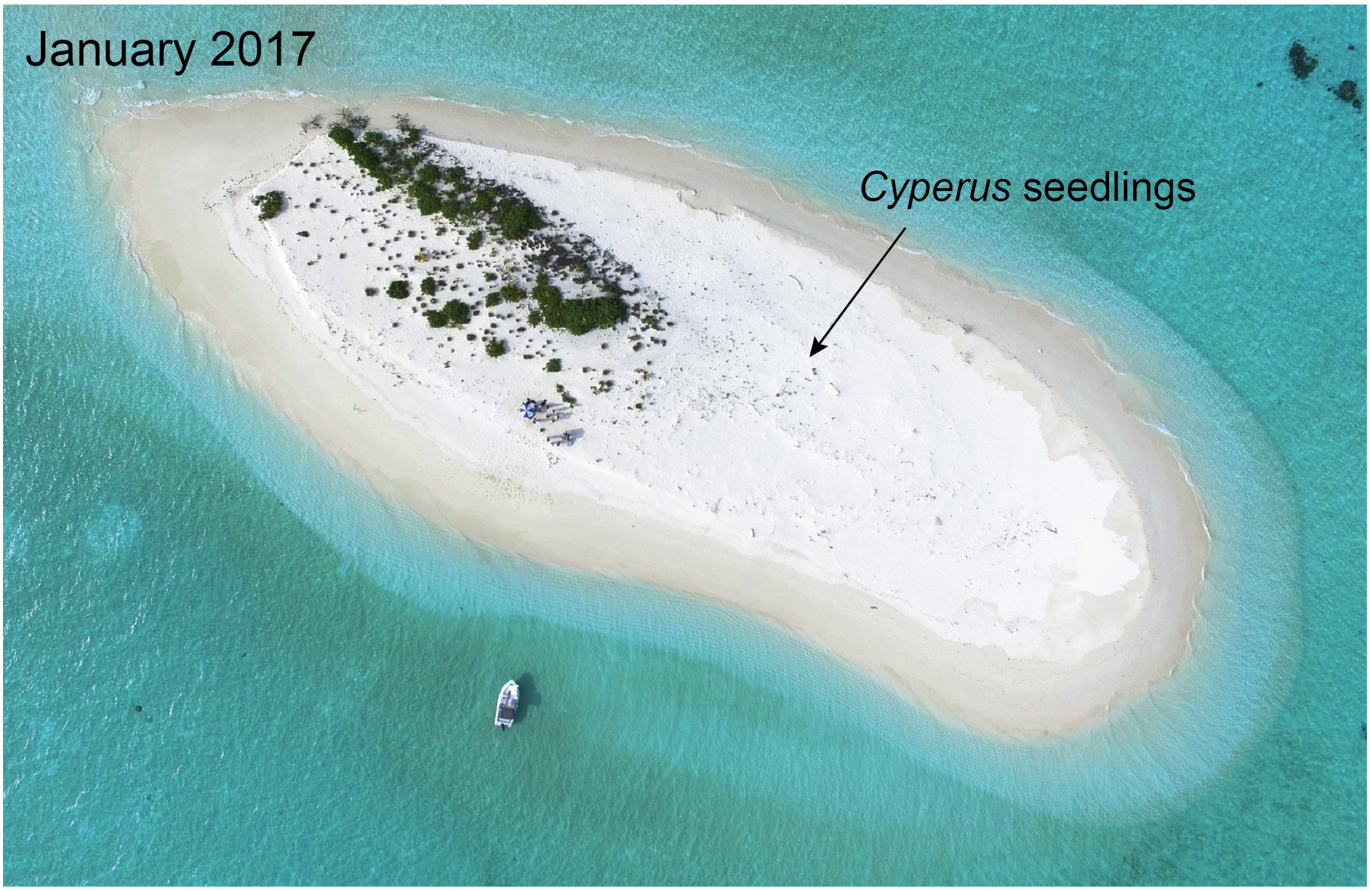
January 2017
Cyperus seedlings

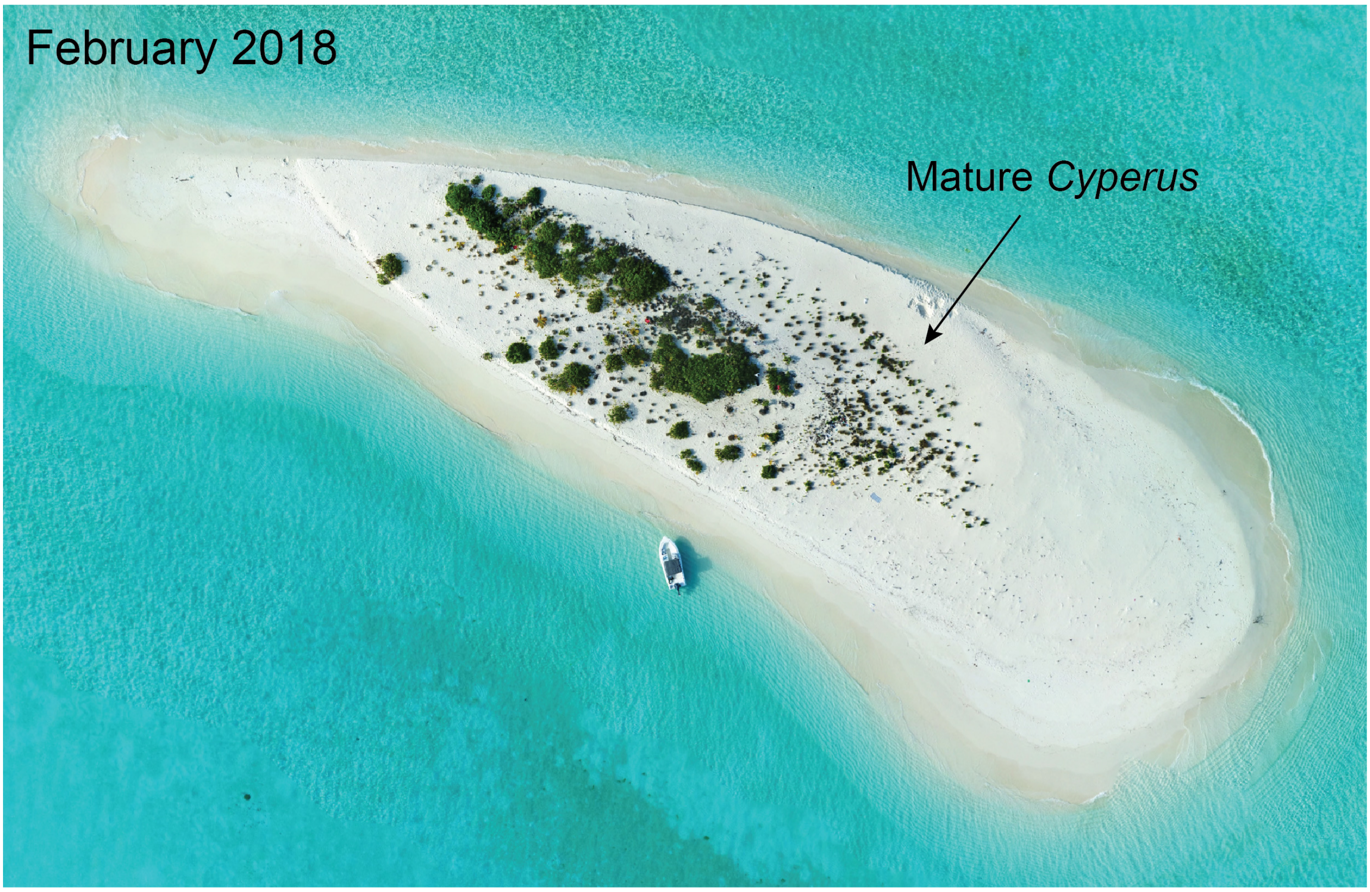
February 2018
Mature Cyperus

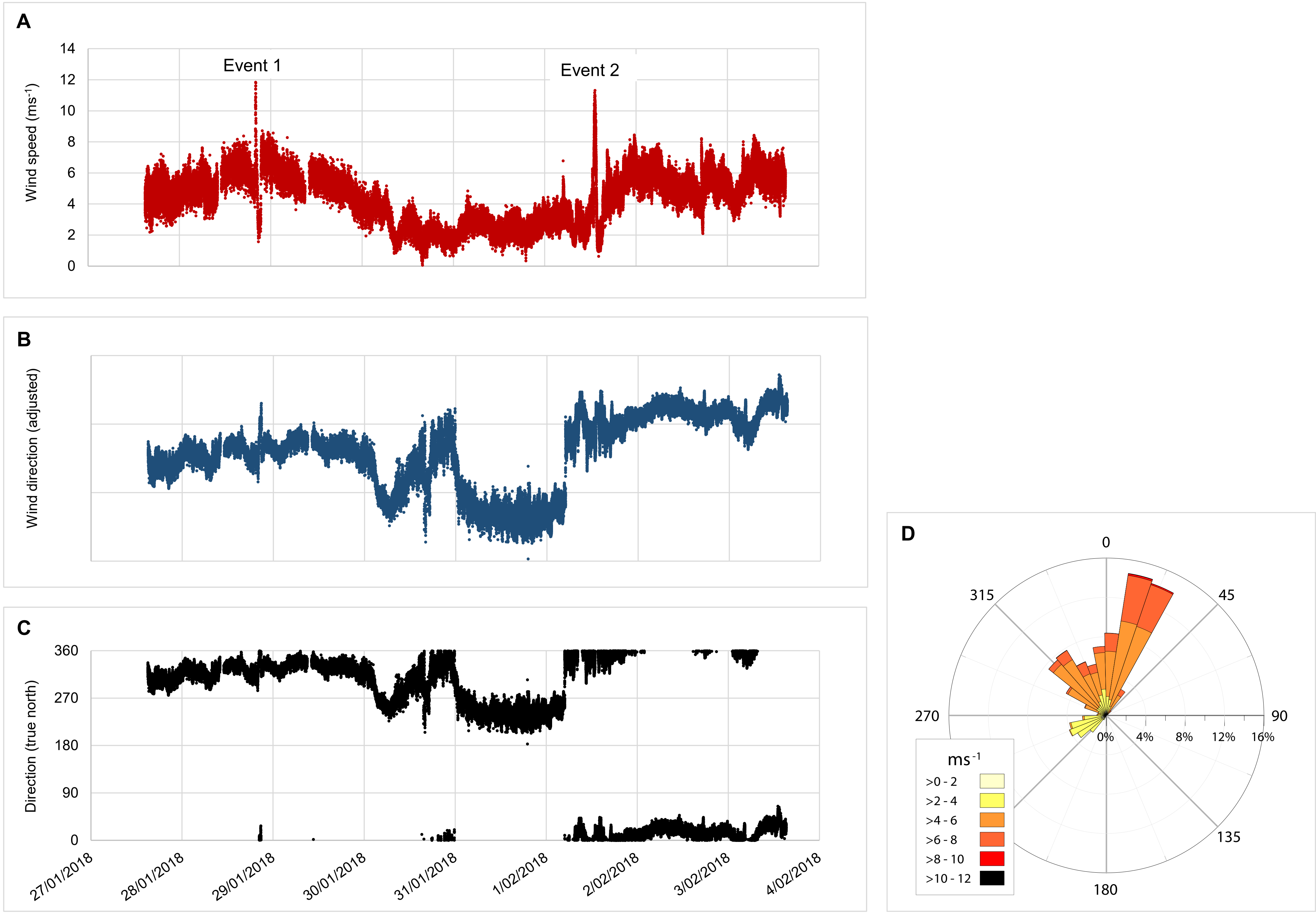

A
Wind speed (ms-1)
0
2
4
6
8
10
12
14
Event 1
Event 2
B
Wind direction (adjusted)
C
Direction (true north)
0
90
180
270
360
27/01/2018
28/01/2018
29/01/2018
30/01/2018
31/01/2018
1/02/2018
2/02/2018
3/02/2018
4/02/2018
D
0
45
90
135
180
270
315
0%
4%
8%
12%
16%
ms-1
>0 - 2
>2 - 4
>4 - 6
>6 - 8
>8 - 10
>10 - 12

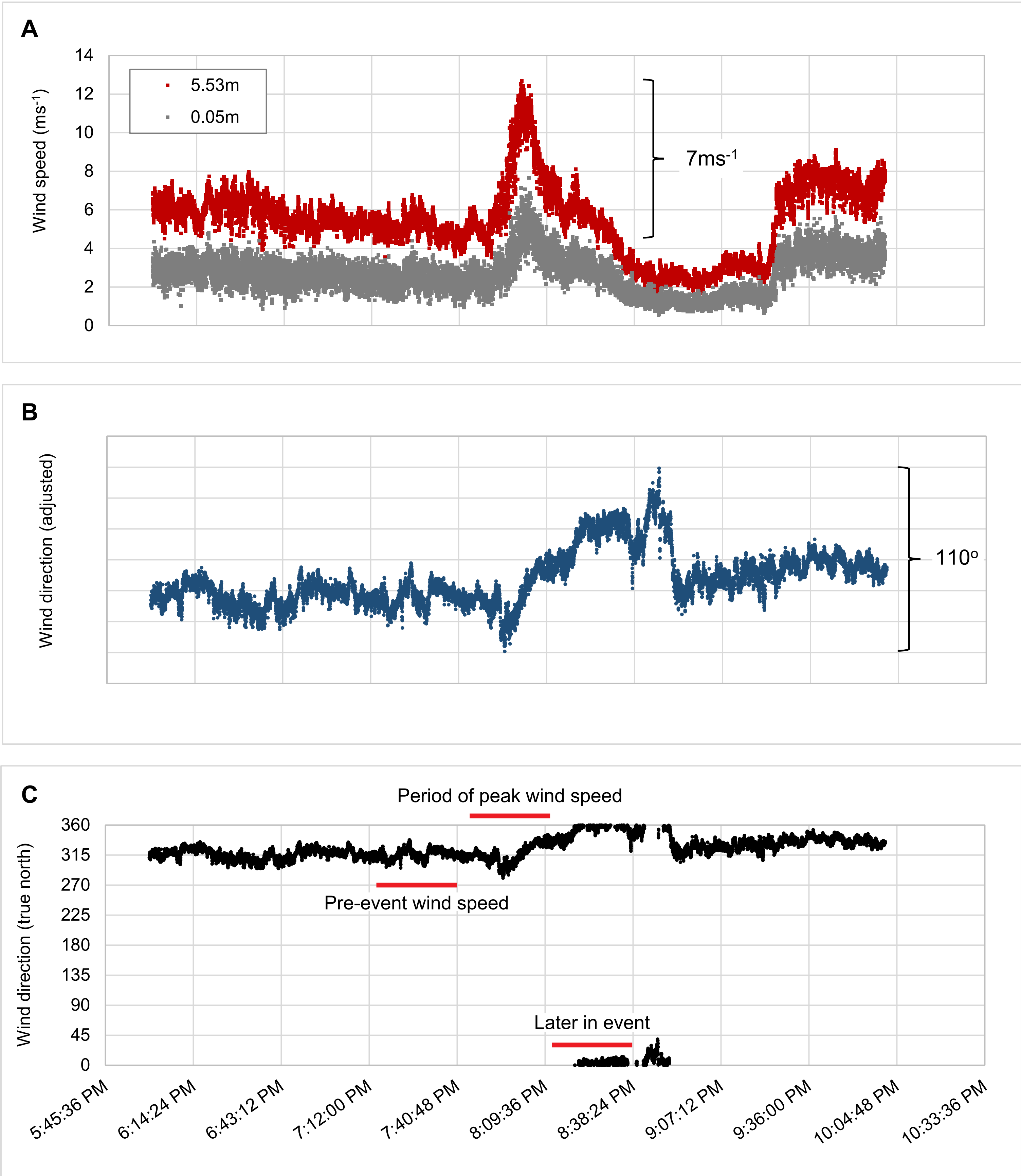

A
Wind speed (ms-1)
14
12
10
8
6
4
2
0
5.53m
0.05m
7ms-1
B
Wind direction (adjusted)
110°
C
Wind direction (true north)
360
315
270
225
180
135
90
45
0
Period of peak wind speed
Pre-event wind speed
Later in event
5:45:36 PM
6:14:24 PM
6:43:12 PM
7:12:00 PM
7:40:48 PM
8:09:36 PM
8:38:24 PM
9:07:12 PM
9:36:00 PM
10:04:48 PM
10:33:36 PM

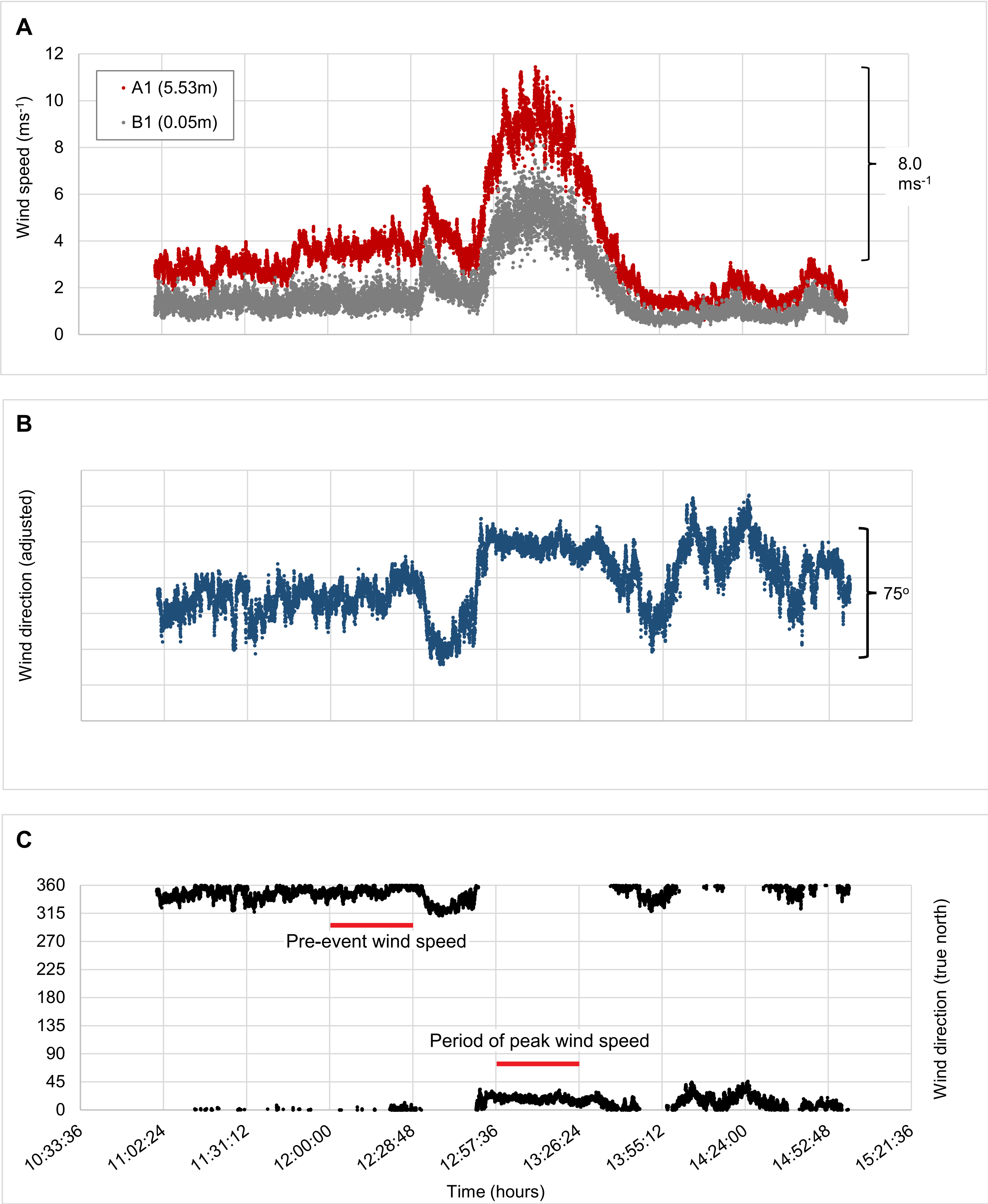

A
Wind speed (ms-1)
12
10
8
6
4
2
0
A1 (5.53m)
B1 (0.05m)
8.0 ms-1
B
Wind direction (adjusted)
75º
C
360
315
270
225
180
135
90
45
0
Pre-event wind speed
Period of peak wind speed
Wind direction (true north)
10:33:36
11:02:24
11:31:12
12:00:00
12:28:48
12:57:36
13:26:24
13:55:12
14:24:00
14:52:48
15:21:36
Time (hours)

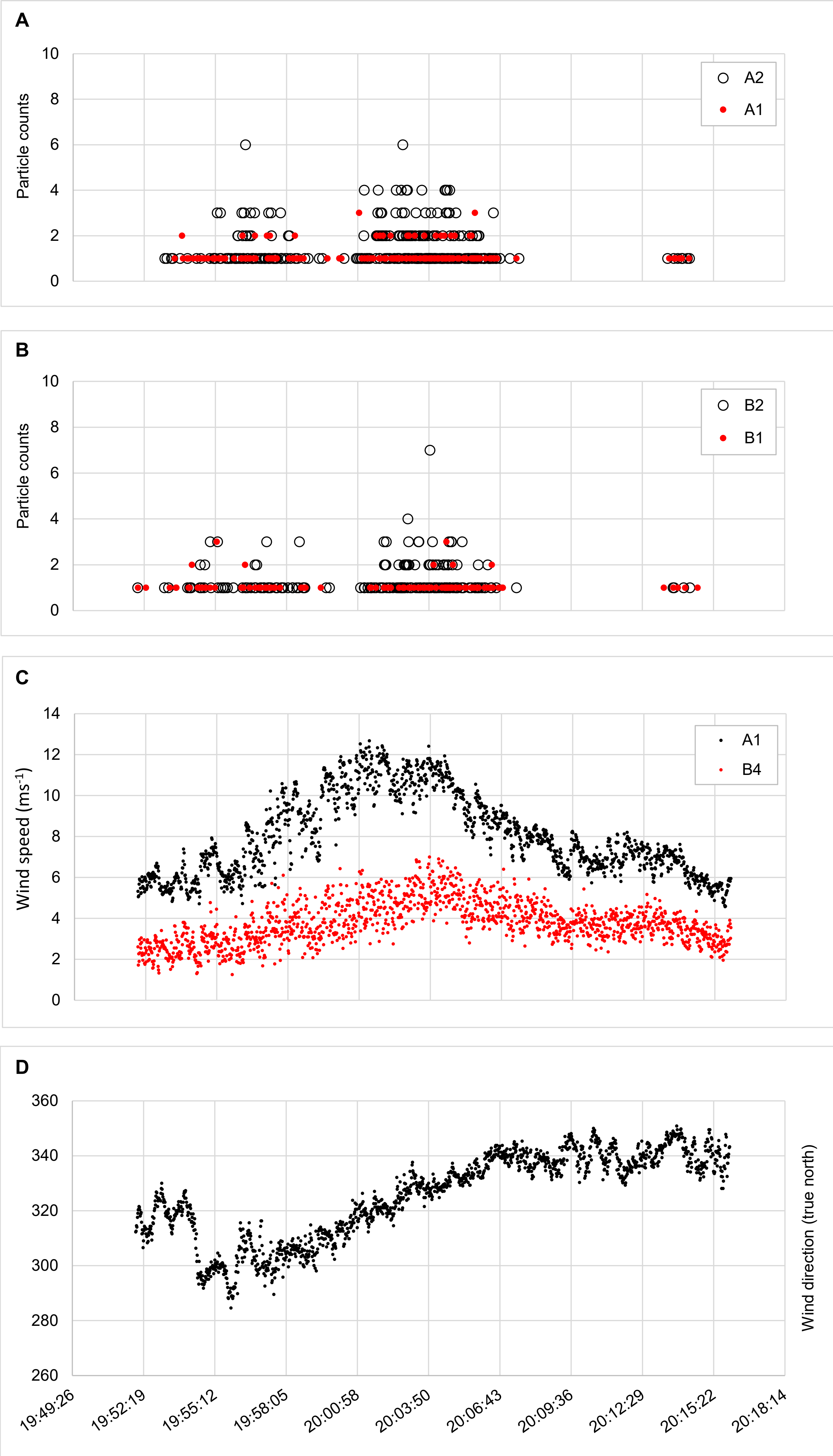

A
Particle counts
0
2
4
6
8
10
A2
A1
B
Particle counts
0
2
4
6
8
10
B2
B1
C
Wind speed (ms-1)
0
2
4
6
8
10
12
14
A1
B4
D
Wind direction (true north)
260
280
300
320
340
360
19:49:26
19:52:19
19:55:12
19:58:05
20:00:58
20:03:50
20:06:43
20:09:36
20:12:29
20:15:22
20:18:14

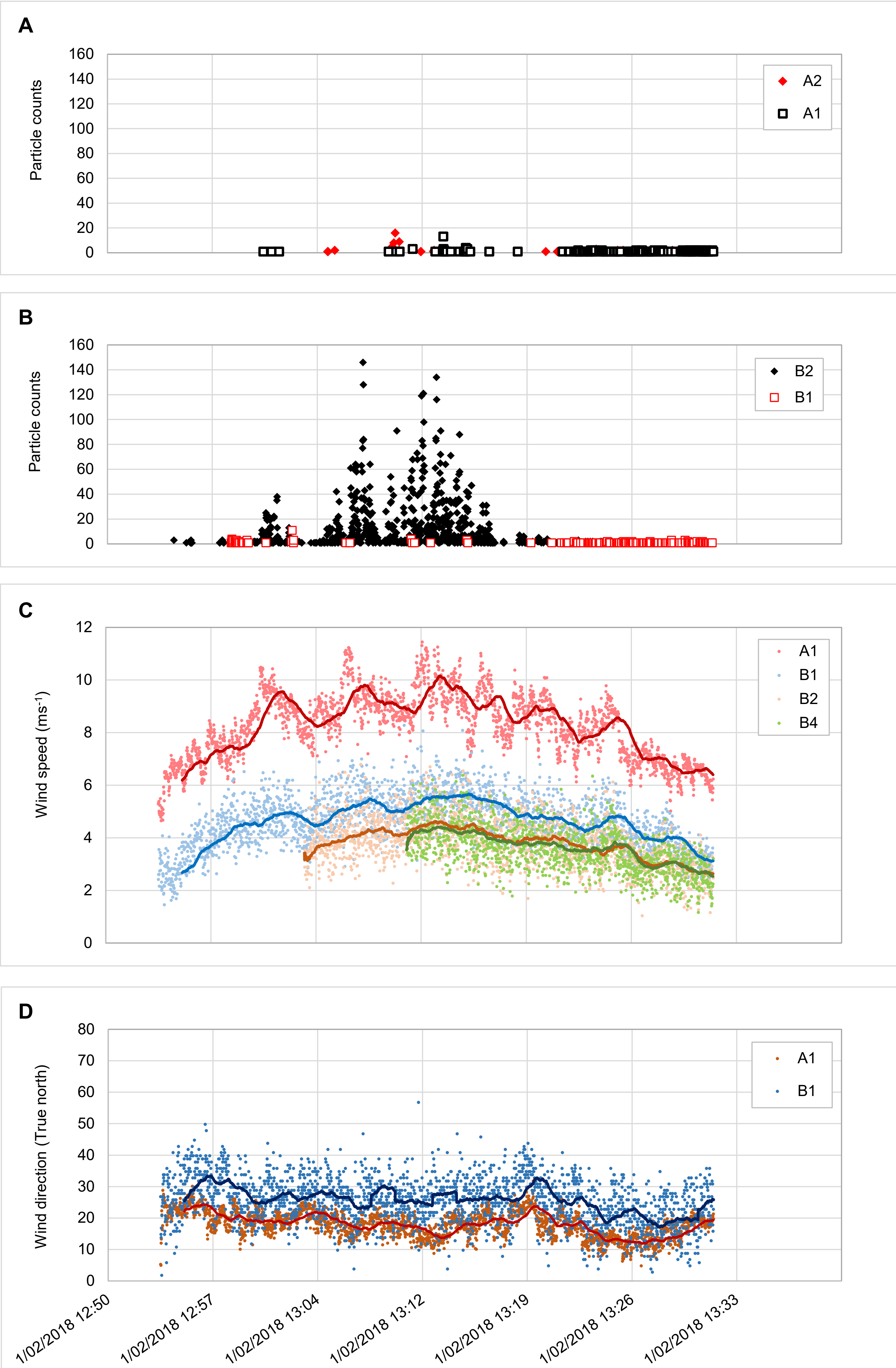
A
Particle counts
A2
A1
B
Particle counts
B2
B1
C
Wind speed (ms^{-1})
A1
B1
B2
B4
D
Wind direction (True north)
A1
B1
1/02/2018 12:50
1/02/2018 12:57
1/02/2018 13:04
1/02/2018 13:12
1/02/2018 13:19
1/02/2018 13:26
1/02/2018 13:33

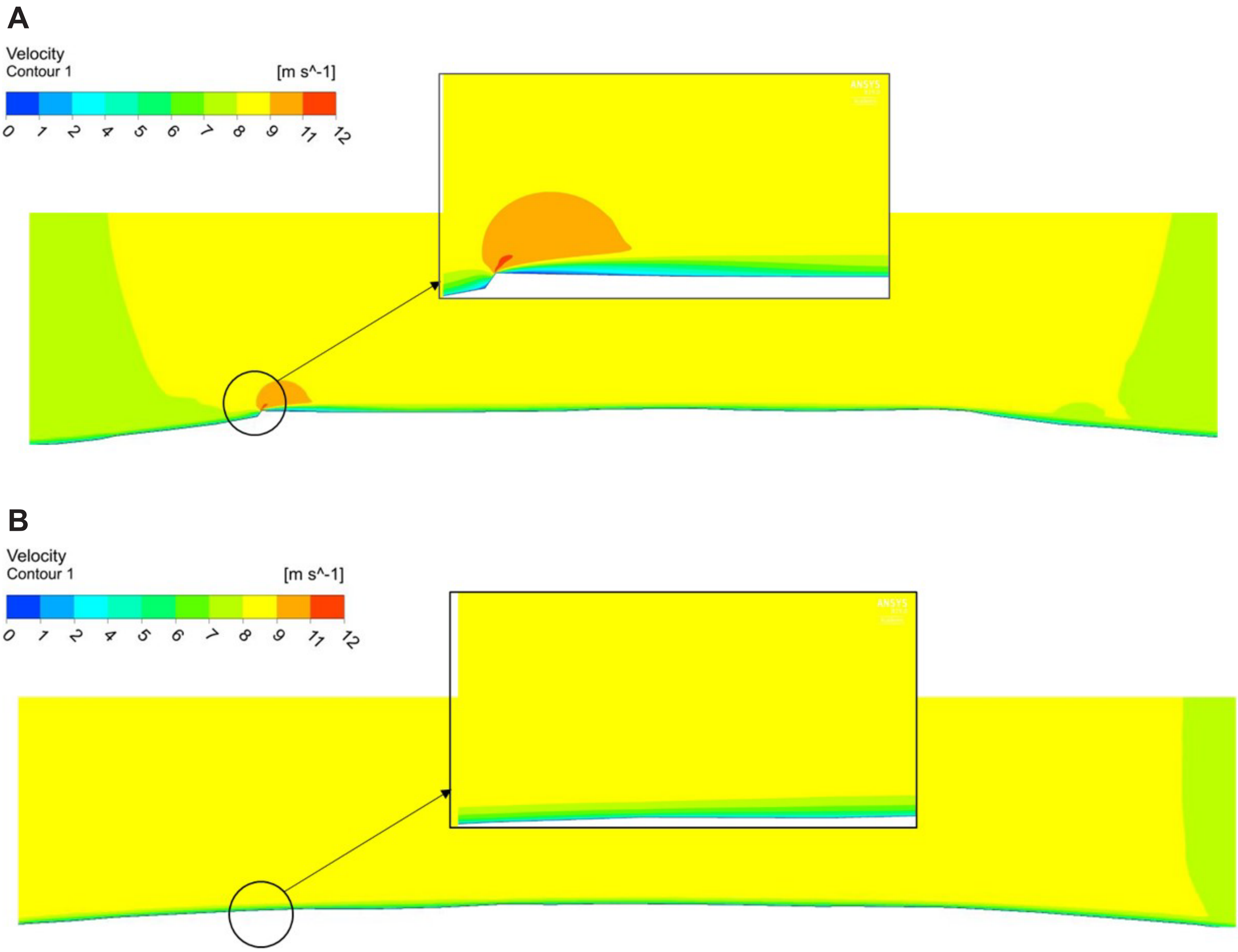
A
Velocity
Contour 1
[m s^-1]
0 1 2 4 5 6 7 8 9 11 12
B
Velocity
Contour 1
[m s^-1]
0 1 2 4 5 6 7 8 9 11 12

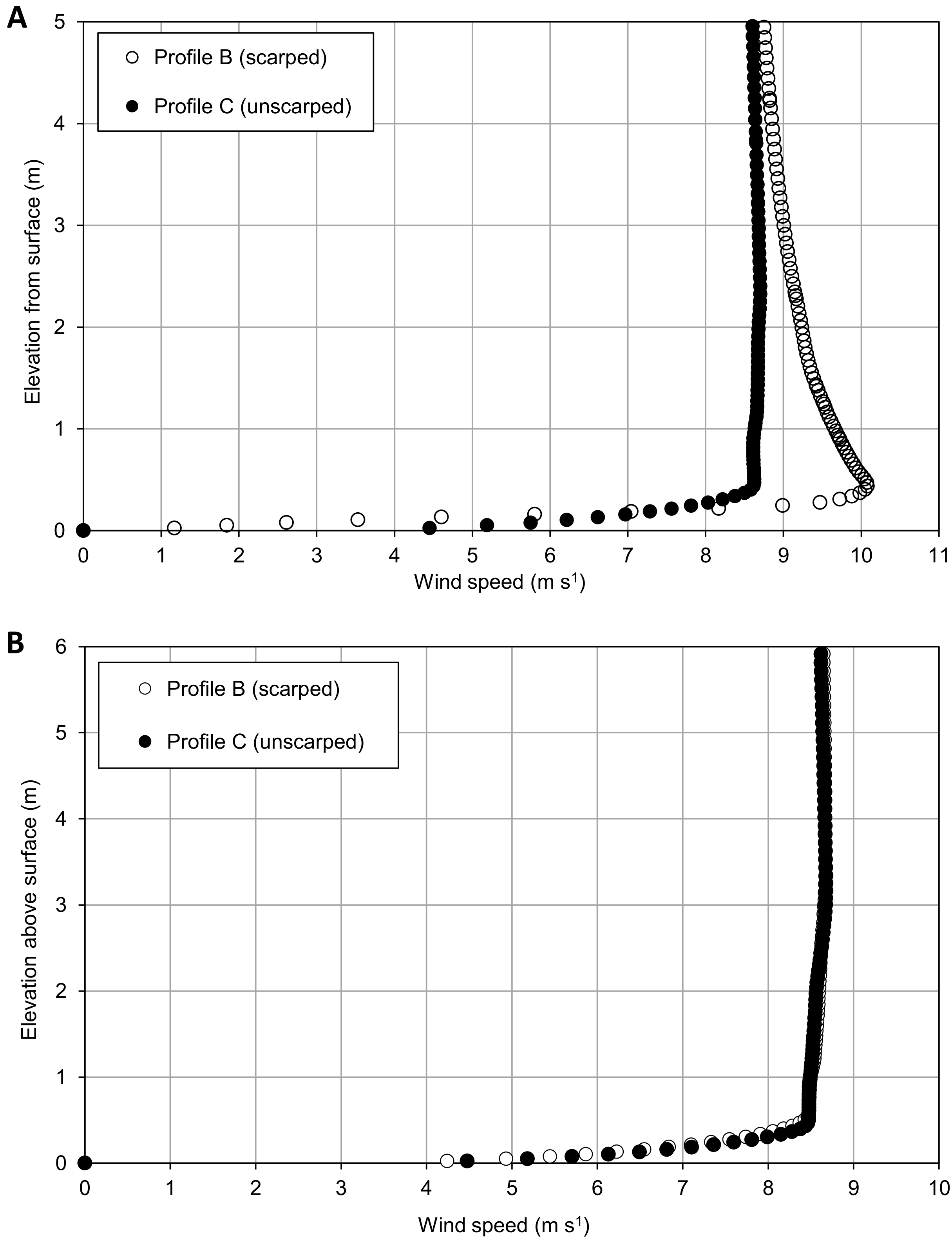
A
Profile B (scarped)
Profile C (unscarped)
Elevation from surface (m)
Wind speed (m s1)
B
Profile B (scarped)
Profile C (unscarped)
Elevation above surface (m)
Wind speed (m s1)

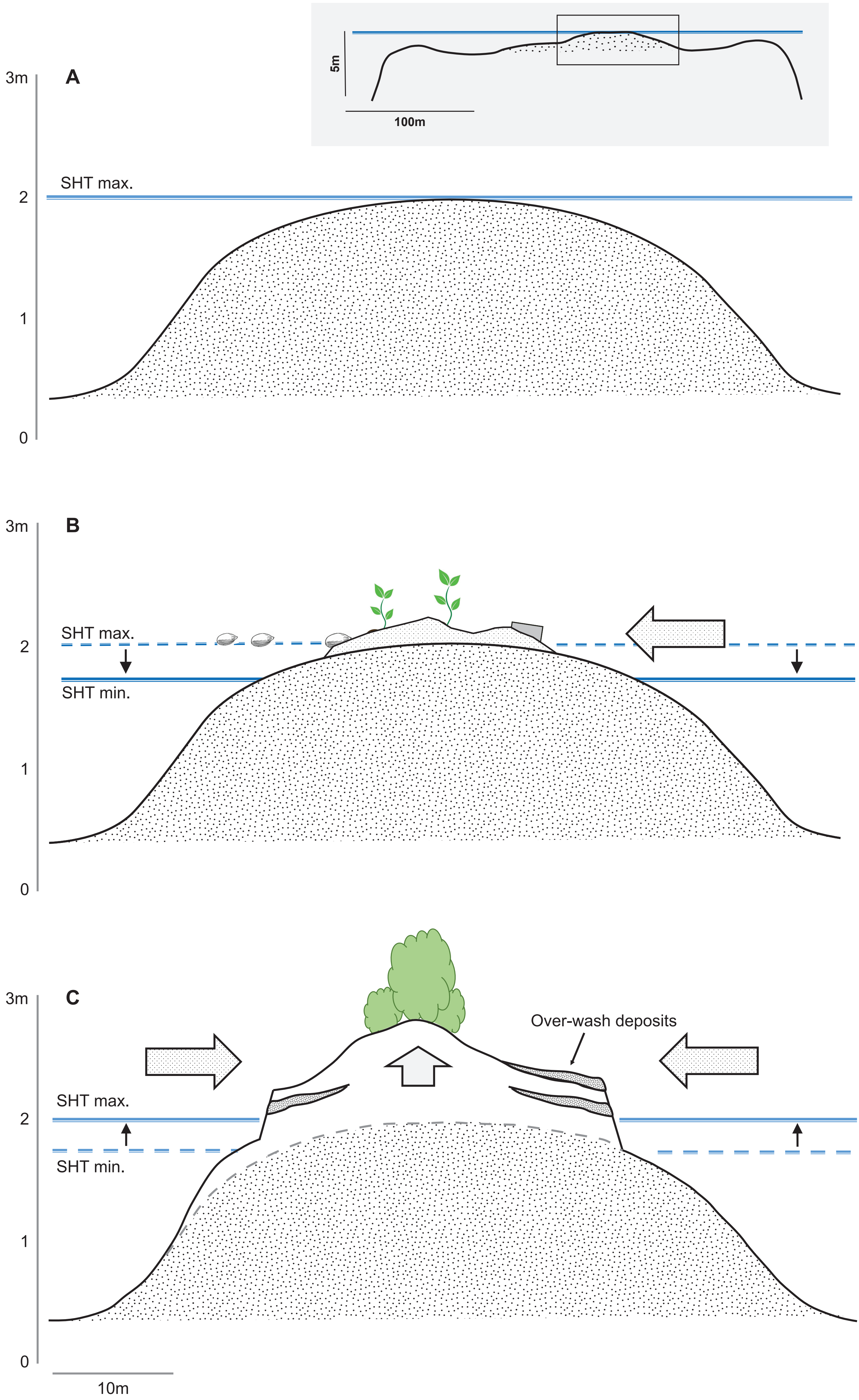

5m
100m
A
3m
2
1
0
SHT max.
B
SHT min.
C
Over-wash deposits
10m

Author contributions:

Hilton, M.J., Borrie, D., Konlechner, T.M., project conceptualisation, fieldwork and data acquisition, funding acquisition, writing

Wakes, S., computational fluid dynamics

Lane, T., data analysis (cloud dynamics) and writing

Mohammed Aslam, fieldwork

Kench, P., fieldwork and writing

Kennedy, D., writing

Author/s:
Hilton, MJ; Borrie, DR; Konlechner, TM; Wakes, SJ; Lane, TP; Kench, PS; Kennedy, DM; Aslam, M

Title:
A first evaluation of the contribution of aeolian sand transport to lagoon island accretion in the Maldives

Date:
2019-08-01

Citation:
Hilton, M. J., Borrie, D. R., Konlechner, T. M., Wakes, S. J., Lane, T. P., Kench, P. S., Kennedy, D. M. & Aslam, M. (2019). A first evaluation of the contribution of aeolian sand transport to lagoon island accretion in the Maldives. Aeolian Research, 39, pp.47-65. https://doi.org/10.1016/j.aeolia.2019.04.006.

Persistent Link:
http://hdl.handle.net/11343/227754

File Description:
Accepted version